Journal of Cosmology and Astroparticle Physics
An IOP and SISSA journal

Hidden charged dark matter

Jonathan L. Feng, Manoj Kaplinghat, Huitzu Tu and Hai-Bo Yu

Department of Physics and Astronomy, University of California,
Frederick Reines Hall, Irvine, California 92697, U.S.A.

E-mail: jlf@uci.edu, mkapling@uci.edu, huitzut@uci.edu, haiboy@uci.edu

Received May 28, 2009
Revised June 11, 2009
Accepted June 11, 2009
Published July 3, 2009

Abstract. Can dark matter be stabilized by charge conservation, just as the electron is in the standard model? We examine the possibility that dark matter is hidden, that is, neutral under all standard model gauge interactions, but charged under an exact U(1) gauge symmetry of the hidden sector. Such candidates are predicted in WIMPless models, supersymmetric models in which hidden dark matter has the desired thermal relic density for a wide range of masses. Hidden charged dark matter has many novel properties not shared by neutral dark matter: (1) bound state formation and Sommerfeld-enhanced annihilation after chemical freeze out may reduce its relic density, (2) similar effects greatly enhance dark matter annihilation in protohalos at redshifts of $z \sim 30$, (3) Compton scattering off hidden photons delays kinetic decoupling, suppressing small scale structure, and (4) Rutherford scattering makes such dark matter self-interacting and collisional, potentially impacting properties of the Bullet Cluster and the observed morphology of galactic halos. We analyze all of these effects in a WIMPless model in which the hidden sector is a simplified version of the minimal supersymmetric standard model and the dark matter is a hidden sector stau. We find that charged hidden dark matter is viable and consistent with the correct relic density for reasonable model parameters and dark matter masses in the range 1 GeV $\lesssim m_X \lesssim$ 10 TeV. At the same time, in the preferred range of parameters, this model predicts cores in the dark matter halos of small galaxies and other halo properties that may be within the reach of future observations. These models therefore provide a viable and well-motivated framework for collisional dark matter with Sommerfeld enhancement, with novel implications for astrophysics and dark matter searches.

Keywords: dark matter theory, galaxy morphology, cosmological perturbation theory

doi:10.1088/1475-7516/2009/07/004

JCAP07(2009)004

Contents

JCAP07(2009)004

1 Introduction

Dark matter makes up most of the matter in the Universe, but its identity is unknown. So far, dark matter has been observed only through its gravitational interactions. A logical possibility, then, is that dark matter is hidden, that is, neutral under all standard model (SM) gauge interactions. This possibility has been explored for many years [1–11] and brings with it a great deal of model building freedom. Unfortunately, this freedom is generically accompanied not only by a loss of predictivity, but also by the loss of appealing features common to other dark matter candidates, such as the strong connections to central problems in particle physics, such as the gauge hierarchy and flavor problems, and the naturally correct thermal relic density of weakly-interacting massive particles (WIMPs).

In this work, we consider the possibility that hidden dark matter is charged under an *exact* U(1) gauge symmetry in the hidden sector. We assume the hidden sector is truly hidden, with no "connector" particles charged under both SM and hidden gauge groups. Although many of our results are relevant for any charged hidden dark matter, including cases with connectors or massive hidden photons, we are particularly motivated by the framework of WIMPless dark matter [12–17], which ameliorates some of the problems of hidden dark matter noted above. (For other recent discussions of hidden dark matter charged under exact gauge symmetries, see refs. [19–21].) In this framework, dark matter is hidden, but additional structure implies that it nevertheless naturally has the correct thermal relic density. In the examples studied in refs. [12–17], the dark matter is in a hidden sector of supersymmetric

models with gauge-mediated supersymmetry breaking (GMSB). Assuming that supersymmetry is broken in a single sector, the hidden sector mass scale m_X and gauge couplings g_X are related to the observable sector weak scale m_W and gauge coupling g_W by

$$\frac{m_X}{g_X^2} \sim \frac{m_W}{g_W^2} \,. \tag{1.1}$$

This implies that the thermal relic density of WIMPless dark matter, $\Omega_X \sim \langle \sigma v \rangle^{-1} \sim m_X^2/g_X^4 \sim m_W^2/g_W^4 \sim \Omega_{\rm WIMP}$, and so is naturally of the desired magnitude, even though m_X need not be at the weak scale. The WIMPless framework also has other virtues, including that fact that it is naturally consistent with an elegant solution to the new physics flavor problem, since the gravitino mass, and with it all dangerous flavor-violating gravity-mediated effects, satisfies $m_{\tilde{G}} \ll m_W$. This contrasts with the case of neutralino dark matter, where stability of the neutralino χ requires $m_{\tilde{G}} > m_\chi \sim m_W$. Other GMSB dark matter candidates have been proposed [22–26]. However, it is notable that the relation $m_X \propto g_X^2$ results directly from the desire to generate a flavor-blind superpartner spectrum. WIMPless dark matter therefore not only dissolves the tension between dark matter and the flavor problem in supersymmetry, but it exploits an elegant solution of the supersymmetric flavor problem to predict the correct thermal relic density.

Assuming $m_{\tilde{G}} < m_X$, however, how is the stability of the hidden sector candidate maintained? Although there are many possibilities in the WIMPless framework [12], an elegant possibility is that the dark matter is charged under an exact gauge symmetry in the hidden sector. The dark matter candidate may then be stable for the same reason that the electron is stable — its decay is prevented by charge conservation. We are therefore led rather straightforwardly to the possibility of charged dark matter in a hidden sector. In the following sections, we will consider, as a concrete example, a minimal supersymmetric standard model (MSSM)-like hidden sector with $\mathcal{O}(1)$ Yukawa couplings. The massless hidden particles — the hidden photon, gluon, and neutrinos — are then all neutral under hidden $\mathrm{U}(1)_{\rm EM}$. Any charged particle in the hidden sector, for example, the hidden W, chargino, stau, tau, or charged Higgs boson, would then be stable, provided it was the lightest m_X particle. A particularly plausible choice is the lighter stau $\tilde{\tau}$, whose mass receives smaller SUSY-breaking contributions than other hidden superparticles.

This possibility of charged hidden dark matter requires a rethinking of many issues in cosmology, as its properties differ markedly from the more conventional possibility of neutral dark matter. In this work, we analyze these issues comprehensively to establish the viability of the scenario and determine what ranges of parameters are allowed. Because the dark matter is charged, it may form bound states and then annihilate in the early Universe. Dark matter annihilation is also enhanced by the Sommerfeld effect [28]. The formation of bound states and the Sommerfeld effect are possible also in the standard model; for example, bound state formation impacts e^+e^- annihilation to 511 keV photons at late times when the e^+ and e^- are non-relativistic. In the present case, both effects may reduce the thermal relic density, potentially destroying the nice relic density property of WIMPless dark matter. After chemical freeze out, the dark matter's charge also plays an important role in kinetic decoupling, since charged dark matter may be far more efficiently coupled to the thermal bath of hidden photons through Compton scattering than neutral dark matter. This impacts the matter power spectrum, requiring a modification of the standard WIMP analysis [29–31]. This also changes the expected minimum mass of dark matter halos. It is important to check the minimum halo mass because the Sommerfeld enhancement charged dark matter annihilation

JCAP07(2009)004

is most effective in the least massive halos where relative velocities are the smallest, and this effect has been noted to provide a stringent constraint on the possibility of charged dark matter [32]. Finally, the existence of a long range force between dark matter particles implies dark matter is collisional. It is therefore also critical to investigate whether this scenario is consistent with constraints on self-interacting dark matter from the Bullet Cluster [33], observed ellipticity of dark matter halos [34] and bounds from considerations of galactic dynamics [19].

In the end, we will find that all of these constraints are satisfied for reasonable model parameters, and are consistent with the correct relic density for dark matter masses in the range 1 GeV $\lesssim m_X \lesssim$ 10 TeV. These dark matter candidates are therefore viable, sharing many of the theoretical virtues of WIMPs, but predicting drastically different features for astrophysics. In its minimal form, this model also predicts no direct detection, indirect detection, and collider signals. If desired, however, with the addition of connector sectors, the charged hidden dark matter model we consider here may also have implications for direct searches, indirect searches, and particle colliders. Some of these implications have been considered previously [12–17], and others are possible [35–50]. We will not expand on these possibilities here, other than to note that our results show that an exact hidden $\mathrm{U}(1)_{\mathrm{EM}}$ is possible, leading to a simple framework in which annihilation rates are enhanced by the pure Sommerfeld effect.

This paper is organized as follows. In section 2, we briefly review our hidden sector model and its parameters, and discuss its thermal relic abundance. In section 3, we study the kinetic decoupling of the hidden sector dark matter, and in section 4 we present the resulting matter power spectrum and derive the minimum mass of dark matter halos. Details of this derivation are given in section A. The impact of bound states and enhanced annihilation on relic densities is evaluated in section 5, and the constraint from annihilation in protohalos is discussed in section 6. In section 7, we study the effect of the long range force between dark matter particles on galaxy shapes and derive bounds on the parameter space. In section 8 we verify that our model is consistent with bounds on self-interactions, such as those from merging clusters. We summarize our conclusions in section 9. We note that this work is necessarily rather wide-ranging; readers interested in only a subset of the topics may find section 9 a useful guide to the relevant conclusions and figures.

2 Hidden sector: particles, parameters, and relic density

In this work, following ref. [16], we consider a hidden sector that is MSSM-like, with gauge group $\mathrm{SU}(3) \times \mathrm{SU}(2)_L \times \mathrm{U}(1)_Y$, but with only one generation of fermions and $\mathcal{O}(1)$ Yukawa couplings. It is important that the model be chiral, so that hidden electroweak symmetry breaking sets the scale for the masses and the naturally correct thermal relic density is realized. Of course, the model should also be anomaly-free. The one-generation MSSM is a relatively simple model that satisfies these criteria, and has the advantage that one can apply much of the intuition built up from studies of the usual MSSM. Many other choices are possible, however, and would also be worth further study. Assuming electroweak symmetry breaking that leaves $\mathrm{SU}(3) \times \mathrm{U}(1)_{\mathrm{EM}}$ preserved in the hidden sector, the particle masses in the hidden sector are

$$\begin{aligned} \text{Hidden weak scale:} \quad & W^h, Z^h, h^h, \tilde{g}^h, \chi^{\pm\, h}, \chi^{0\, h}, t^h, b^h, \tau^h, \tilde{t}^h, \tilde{b}^h, \tilde{\tau}^h, \tilde{\nu}^h_\tau \\ \sim 0: \quad & \gamma^h, g^h, \nu^h_\tau, \tilde{G}\,, \end{aligned} \tag{2.1}$$

JCAP07(2009)004

where we have used third-generation notation for the hidden (s)quarks and (s)leptons to remind us that they have $\mathcal{O}(1)$ Yukawa couplings. From this spectrum, a natural possibility is that the lightest weak scale particle is charged, and therefore stabilized by $\mathrm{U}(1)_{\mathrm{EM}}$ charge conservation in the hidden sector. As noted in section 1, there are many possible charged dark matter candidates in the hidden sector. To be concrete, we will focus here on the right-handed stau, which we denote $\tilde{\tau}^h$ from now on.

Despite the complexity of the hidden sector, with a few mild assumptions, there are only a few parameters that are relevant for this study. These are

$$m_X,\ m_{Z^h},\ \alpha_X,\ \tan\theta_W^h,\ \xi_{\mathrm{RH}} \equiv \frac{T_{\mathrm{RH}}^h}{T_{\mathrm{RH}}}\,, \tag{2.2}$$

where $m_X = m_{\tilde{\tau}^h}$ is the dark matter particle's mass, m_{Z^h} is the mass of the hidden Z boson, $\alpha_X = (e^h)^2/4\pi$ is the fine structure constant of the hidden $\mathrm{U}(1)_{\mathrm{EM}}$, θ_W^h is the hidden sector's weak mixing angle, and ξ_{RH} is the ratio of hidden to observable sector temperatures at the time of reheating. The parameter ξ_{RH} need not be 1; for example, the inflaton may couple differently to the observable and hidden sectors, leading to a temperature asymmetry [3, 4]. For a one-generation MSSM to satisfy Big Bang nucleosynthesis constraints on massless degrees of freedom, one requires $\xi_{\mathrm{RH}} \lesssim 0.8$ [16]. We will consider values in the range $0.1 \leq \xi_{\mathrm{RH}} \leq 0.8$. In the hidden sector, the γ^h and ν^h temperatures are always identical, and we denote the common temperature by T^h. In the visible sector, the γ and ν temperatures diverge eventually, of course; we denote let T denote the γ (cosmic microwave background (CMB)) temperature. We do not assume hidden sector gauge unification, although we will present some of our results for the grand unified value $\tan\theta_W^h = \sqrt{3/5} \simeq 0.8$ as an interesting example. We assume that the hidden sector's strong coupling g_s is small enough that hadronization effects are negligible in the early Universe.

The hidden dark matter's relic abundance is determined by the parameters of eq. (2.2). The dark matter annihilates through $\tilde{\tau}^{h+}\tilde{\tau}^{h-} \to \gamma^h\gamma^h, \nu^h\bar{\nu}^h$. If the $\tilde{\tau}^h$ is dominantly right-handed, its thermally-averaged annihilation cross section is [16]

$$\langle\sigma_A v\rangle(T^h) = \frac{(4\pi\alpha_X)^2}{m_X^2}\left[a_0 + a_1\frac{T^h}{m_X} + \mathcal{O}\left(\frac{T^h}{m_X}\right)^2\right], \tag{2.3}$$

where

$$\begin{aligned} a_0 &= \left[\frac{1}{8\pi} + \frac{1}{4\pi}\left(1 - \frac{m_{Z^h}^2}{4m_X^2}\right)\tan^2\theta_W^h\right] \\ a_1 &= -\frac{1}{4\pi} - \frac{1}{2\pi}\tan^2\theta_W^h + \frac{1}{8\pi}\frac{1}{\cos^4\theta_W^h\left[\left(-4 + \frac{m_{Z^h}^2}{m_X^2}\right)^2 + \frac{m_{Z^h}^2\Gamma_{Z^h}^2}{m_X^4}\right]}\,. \end{aligned} \tag{2.4}$$

To avoid presenting results for the special case in which the annihilation cross section is resonantly enhanced by the Z^h pole, we fix $m_{Z^h} = 1.5m_X$. The dependence of $\langle\sigma_A v\rangle$ on Γ_{Z^h} is therefore negligible. In the numerical studies below, we will consider weak mixing angles in the range $\sqrt{3/5} \leq \tan\theta_W^h \leq 10$. If the hidden sector has custodial symmetry, $m_{W^h} = m_{Z^h}\cos\theta_W^h$, then $\tan\theta_W^h > 1.11$ implies $m_{W^h} < m_{\tilde{\tau}^h}$. Although W^h would also be a perfectly good charged hidden dark matter candidate, we will instead assume custodial

JCAP07(2009)004

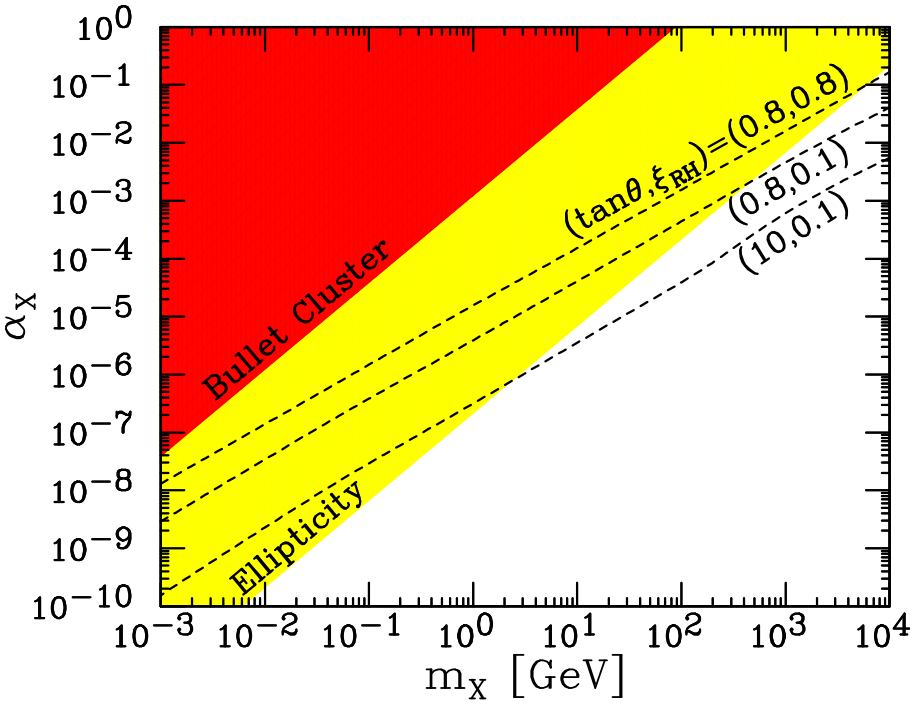

Figure 1. Allowed regions in (m_X, α_X) plane, where m_X is the mass of the dark matter charged under the unbroken hidden sector $\mathrm{U}(1)_{\mathrm{EM}}$ with fine-structure constant α_X. Contours for fixed dark matter cosmological relic density consistent with WMAP results, $\Omega_X h^2 = 0.11$, are shown for $(\tan\theta_W^h, \xi_{\mathrm{RH}}) = (\sqrt{3/5}, 0.8)$, $(\sqrt{3/5}, 0.1)$, $(10, 0.1)$ (dashed), from top to bottom, as indicated. The shaded regions are disfavored by constraints from the Bullet Cluster observations on self-interactions (dark red) and the observed ellipticity of galactic dark matter halos (light yellow). The Bullet Cluster and ellipticity constraints are derived in sections 8 and 7, respectively.

symmetry is broken, for example, by triplet Higgs bosons, so that $\tilde{\tau}^h$ remains the dark matter candidate for all values of $\tan\theta_W^h$.

With these assumptions, contours of constant $\Omega_X h^2$ in the (m_X, α_X) plane are given in figure 1. (Constraints from observations are also shown in figure 1; these will be discussed in sections 7 and 8.) As evident from figure 1 and eq. (2.4), there is a strong dependence on $\tan\theta_W^h$: for fixed α_X, the neutrino cross section is enhanced by $1/\cos^4\theta_W^h$ for large $\tan\theta_W^h$. This dependence is very important. In high energy processes, such as thermal freeze out, both EM and weak processes are effective. In low energy processes, such as those occurring at present, only EM interactions mediated by the massless γ^h are important. If there were no hidden weak interactions, for fixed m_X and ξ_{RH}, $\Omega_X h^2 \simeq 0.11$ would fix α_X, and so the relic density would fix the strength of dark matter self-interactions now. In the more general case we are considering, however, one can keep Ω_X constant for arbitrarily small α_X, provided $\tan\theta_W^h$ is large enough. As noted above, we will consider $\tan\theta_W^h$ as large as 10; larger values are, of course, also possible.

3 Kinetic decoupling of dark matter

In the standard cosmology, structure formation is hierarchical, that is, small objects form first and progressively the larger objects form via mergers and accretion. The mass of the smallest

JCAP07(2009)004

dark matter halo is determined by the dark matter particle's mass and the temperature at which it kinetically decouples from the other light particle species. For a typical WIMP with electroweak scale mass, the kinetic decoupling temperature ranges roughly from 10 MeV to 1 GeV, which leads to the formation of dark matter halos with masses as small as $10^{-12} M_\odot$ to $10^{-4} M_\odot$ [29–31, 51–55]. For other dark matter particles, such as weak-scale gravitinos or MeV dark matter, the minimum mass dark matter halo could be as large as the smallest dwarf galaxies [56–58]. Some regions of the parameter space of these models are excluded because the predicted minimum mass halo is in conflict with observations.

In this section, we analyze the kinetic decoupling of hidden charged dark matter. One notable difference between the WIMP and hidden charged dark matter is that the charged dark matter interacts not only through weak interactions, but also through EM interactions. For the case of $\tilde{\tau}^h$ dark matter, this implies that the dark matter remains in kinetic contact not only through the weak process $\tilde{\tau}^h \nu^h \leftrightarrow \tilde{\tau}^h \nu^h$, but also through the Compton scattering process $\tilde{\tau}^h \gamma^h \leftrightarrow \tilde{\tau}^h \gamma^h$. As we will see, at low temperatures, the thermally-averaged weak cross section is suppressed by $T^{h\,2}/m_X^2$, but this suppression is absent for Compton scattering, creating a large, qualitative difference between this case and the canonical WIMP scenario. Note also that, in principle, in the case of charged dark matter, bound state formation also impacts kinetic decoupling. As we will see in section 5, however, very few staus actually bind, and so this effect is not significant and may be neglected in our analysis.

We follow refs. [54, 55] to determine the temperature of kinetic decoupling for the dark matter particle. In the hidden sector, the Boltzmann equation governing the evolution of the dark matter particle's phase space distribution is

$$\frac{df(\vec{p})}{dt} = \Gamma(T^h)(T^h m_X \triangle_{\vec{p}} + \vec{p} \cdot \nabla_{\vec{p}} + 3) f(\vec{p}) \,, \tag{3.1}$$

where

$$\Gamma(T^h) = \sum_n \frac{g_0}{6(2\pi)^3} m_X c_n N_{n+3}^{\pm} \left(\frac{T^h}{m_X}\right)^{n+4} \tag{3.2}$$

is the momentum transfer rate. In eq. (3.2), g_0 is the number of degrees of freedom of the scattering particle ($g_0 = 2$ for both γ^h and ν^h), the $N_{n+3}^{\pm}$ are constants defined in ref. [55], and the c_n are determined by parameterizing the collision amplitudes, evaluated at $t = 0$ and $s = m_X^2 + 2 m_X T^h$, as

$$|\mathcal{M}|^2_{t=0, s=m_X^2+2m_X T^h} \equiv c_n \left(\frac{T^h}{m_X}\right)^n + \mathcal{O}\left(\frac{T^h}{m_X}\right)^{n+1} . \tag{3.3}$$

In the present case, with the help of the CalcHEP program [59, 60], we find that the squared amplitudes of the relevant processes are

$$\left|\mathcal{M}(\tilde{\tau}^h \gamma^h \leftrightarrow \tilde{\tau}^h \gamma^h)\right|^2 = \frac{64\pi^2 \alpha_X^2 \left[(m_X^2 - s)^4 + 2(m_X^2 - s)^2 st + (m_X^4 + s^2) t^2\right]}{(m_X^2 - s)^2 (-m_X^2 + s + t)^2} \tag{3.4}$$

$$\left|\mathcal{M}(\tilde{\tau}^h \nu^h \leftrightarrow \tilde{\tau}^h \nu^h)\right|^2 = \frac{16\pi^2 \alpha_X^2 \left[(m_X^2 - s)^2 + st\right]}{\cos^4 \theta_W^h \, (m_Z^2 - t)^2} , \tag{3.5}$$

and so

$$\left|\mathcal{M}(\tilde{\tau}^h \gamma^h \leftrightarrow \tilde{\tau}^h \gamma^h)\right|^2_{t=0, s=m_X^2+2m_X T^h} = 64\pi^2 \alpha_X^2 \tag{3.6}$$

$$\left|\mathcal{M}(\tilde{\tau}^h \nu^h \leftrightarrow \tilde{\tau}^h \nu^h)\right|^2_{t=0, s=m_X^2+2m_X T^h} = \frac{64\pi^2 \alpha_X^2 m_X^4}{\cos^4 \theta_W^h m_Z^4} \left(\frac{T^h}{m_X}\right)^2 . \tag{3.7}$$

JCAP07(2009)004

Casting these results in the form of eq. (3.3), we find

$$\Gamma(T^h) = \frac{32\pi^3\alpha_X^2\, T^{h\,4}}{45\, m_X^3} + \frac{124\pi^5\alpha_X^2\, m_X\, T^{h\,4}}{63\cos^4\theta_W^h\, m_Z^4}\left(\frac{T^h}{m_X}\right)^2 . \tag{3.8}$$

The inverse of $\Gamma(T^h)$ is the time needed for the hidden sector photons and neutrinos to transfer momentum $|\vec{p}| \sim T^h$ to the staus and thereby keep the dark matter in kinetic equilibrium. During this phase, the temperature of the dark matter tracks that of the hidden section photons or neutrinos, depending on the dominant scattering mechanism. The contribution from Compton scattering (the first term) does not suffer the $(T^h/m_X)^2$ suppression typical of weak interactions. Therefore, for $\tan\theta_W^h \sim 1$, Compton scattering dominates the contribution to $\Gamma(T^h)$. However, for $\tan\theta_W^h = 10$, the ν^h channel is enhanced dramatically and dominates for $m_X \lesssim 1$ GeV.

We define the kinetic decoupling temperature as the temperature where the momentum transfer rate and the Hubble expansion rate become equal, that is, $\Gamma(T^h_{\rm kd}) = H(T^h_{\rm kd})$. (For other possible definitions, see, for example, refs. [54, 55].) Here we adopt the hidden sector point of view and write the Hubble parameter as

$$H(T^h) = \sqrt{\frac{4\pi^3}{45} g_*^{\rm tot}(T^h)}\,\frac{T^{h\,2}}{M_{\rm pl}}\,, \tag{3.9}$$

where $g_*^{\rm tot}(T^h) = g_*^h + g_*\left(T/T^h\right)^4$ is the total effective relativistic degrees of freedom, and T is the visible sector's photon temperature. We assume there is no thermal contact between hidden and observable sectors, and so the visible sector enters the analysis only through the contribution of its effective degrees of freedom g_* to the expansion rate.

In figure 2 we show the hidden sector kinetic decoupling temperature $T^h_{\rm kd}$ and visible sector kinetic decoupling temperature $T_{\rm kd}$ as functions of m_X for various combinations of $(\tan\theta_W^h, \xi_{\rm RH})$. The hidden $\mathrm{U}(1)_{\rm EM}$ fine-structure constant α_X is determined by requiring the correct dark matter relic abundance $\Omega_X h^2 = 0.11$. To understand these results, consider first the case $(\tan\theta_W^h, \xi_{\rm RH}) = (\sqrt{3/5}, 0.8)$ and $m_X \sim 100$ GeV. In this case, $g_1 \sim g_2$ in the hidden sector, the hidden and observable sectors have comparable temperatures, and the dark matter has a weak-scale mass. This case is thus similar to the standard WIMP case, except that the hidden dark matter is charged. For the WIMP case, one typically finds $T_{\rm kd} \sim 10\,\mathrm{MeV}{-}1$ GeV, as noted above, whereas in this charged hidden dark matter case, we find that $T_{\rm kd} \sim 0.1$ MeV. We see that the presence of Compton scattering does in fact have a large impact, keeping the charged dark matter in kinetic equilibrium to much lower temperatures.

This effect is moderated for other values of $(\tan\theta_W^h, \xi_{\rm RH})$. For $(\tan\theta_W^h, \xi_{\rm RH}) = (\sqrt{3/5}, 0.1)$, the hidden sector is colder relative to the visible sector. As shown in ref. [16], a colder hidden sector requires a smaller α_X to meet the relic abundance constraint, which results in a smaller momentum transfer rate. Furthermore, for a colder hidden sector, the visible sector appears hotter. The resulting larger Hubble expansion rate of eq. (3.9) also causes the momentum transfer processes to become inefficient earlier. This effect is even more pronounced for $(\tan\theta_W^h, \xi_{\rm RH}) = (10, 0.1)$, since large $\tan\theta_W^h$ implies even lower α_X, increasing the visible sector $T_{\rm kd}$ further.

4 Power spectrum of dark matter density fluctuations

The interactions and subsequent decoupling of dark matter particles damp the matter power spectrum. The matter power spectrum is the Fourier transform of the two-point function of

JCAP07(2009)004

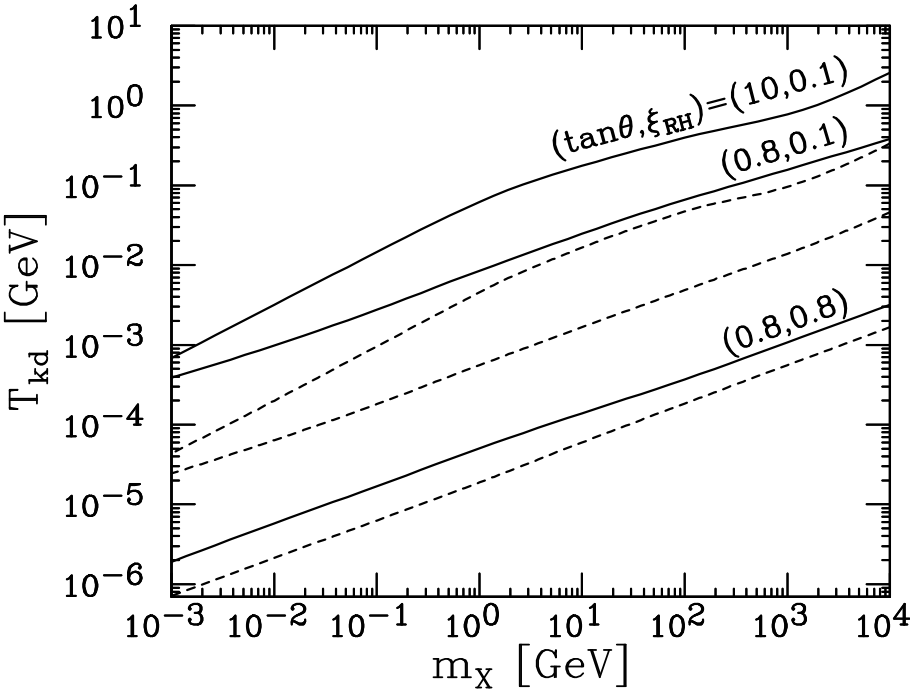

Figure 2. Kinetic decoupling temperatures as functions of dark matter mass m_X for $(\tan\theta_W^h, \xi_{\rm RH}) = (10, 0.1)$, $(\sqrt{3/5}, 0.1)$, $(\sqrt{3/5}, 0.8)$, from top to bottom, as indicated. For each case we plot both the hidden sector photon temperature $T_{\rm kd}^h$ (dashed) and the corresponding visible sector photon (CMB) temperature $T_{\rm kd}$ (solid) at the time of kinetic decoupling.

the cosmological density fluctuations in matter. For Gaussian initial conditions, this encodes all the relevant information for linear perturbation theory. In this section, we will study the power spectrum of hidden charged dark matter to contrast its predictions with that of canonical WIMP models. We will focus on small scales where differences might be expected, especially in the predictions for the mass of the smallest dark matter structures that can form. We will find that the differences from the usual WIMP models are not observable with current data, although these may be observable in the future. However, the smallest halo mass prediction is important for the calculation of Sommerfeld-enhanced self-annihilations, which we will discuss in the following section.

The damping due to the coupling of charged dark matter to hidden sector photons (and neutrinos) results from two distinct processes. The coupling of the dark matter to the hidden sector photons and neutrinos leads to damped oscillatory features [52] due to the interplay between the gravity of dark matter and the pressure of the photons. This is the dominant effect for the case of WIMPs with electroweak scale masses and also for our case with $m_X > 1$ GeV. In addition, after decoupling, the free-streaming of the dark matter particles further suppresses the power spectrum. This effect dominates at lower masses and in particular in the region of parameter space where interactions with the hidden sector neutrinos dominate over those with hidden sector photons.

The presence of the hidden sector and the coupling of the dark matter to γ^h and ν^h make the decoupling and matter power spectrum calculation different from the standard WIMP case. The two main differences are the following. In the standard WIMP case, the

JCAP07(2009)004

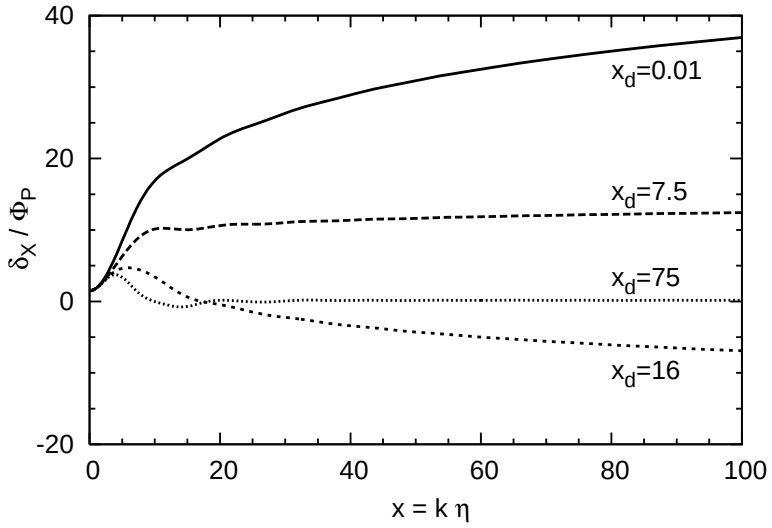

Figure 3. The normalized amplitudes of dark matter fluctuation for different modes with comoving wavenumbers $x_d = 0.01, 7.5, 75, 16$ as functions of $x = k\eta$, where η is the conformal time. We fix $(\tan\theta_W^h, \xi_{\rm RH}) = (\sqrt{3/5}, 0.8)$ for this plot.

WIMP couples to standard model fermions that are part of a tightly coupled (collisionally-coupled) fluid. This implies that multipole moments of the density fluctuations higher than the dipole are strongly suppressed. This result stems from the fact that in a collisionally-coupled plasma, a quadrupole anisotropy pattern can only develop if there is significant diffusion. In the present case, the hidden sector photons and neutrinos are only coupled to the dark matter and are able to diffuse significantly. We therefore need to track their density fluctuations to higher multipoles. The other notable difference is that the expansion rate is predominantly set by the visible sector matter and so the ratio of the scattering rate in the hidden sector to expansion rate is different from the usual WIMP case. We provide details about this calculation in appendix A.

In figure 3 we show the normalized density fluctuations for different modes as functions of $x = k\eta$, where η is the conformal time. The coupling between $\tilde{\tau}^h$ and γ^h results in damped oscillations as mentioned previously, and this is apparent in figure 3 for the modes that enter the horizon before kinetic decoupling. However, there is one major difference between this hidden sector scenario and the WIMP scenario studied in refs. [52, 54]: the oscillation amplitude is much smaller than it is in the WIMP case. This traces back to the $\tilde{\tau}^h\gamma^h$ scattering cross section, which is $\sim \alpha_X^2/m_X^2 \sim g_W^4/m_W^2$, that is, set by the SM weak scale, which is far smaller than the analogous visible sector cross section, which is the Thomson cross section $\sim g_W^4/m_e^2$. The smaller opacity in the hidden sector case results in large diffusion damping and hence the oscillations are highly suppressed.

In figure 4 we plot transfer functions of the density perturbation of the hidden charged dark matter for various m_X and combinations of $(\tan\theta_W^h, \xi_{\rm RH})$. For smaller masses, kinetic decoupling happens later and the matter power spectrum is more suppressed. We define the cut-off wavenumber $k_{\rm cut}$ as the point where the transfer function first drops to $1/e$ of its value at small wavenumbers. For $(\tan\theta_W^h, \xi_{\rm RH}) = (\sqrt{3/5}, 0.8)$ (top panel) and $m_X =$

JCAP07(2009)004

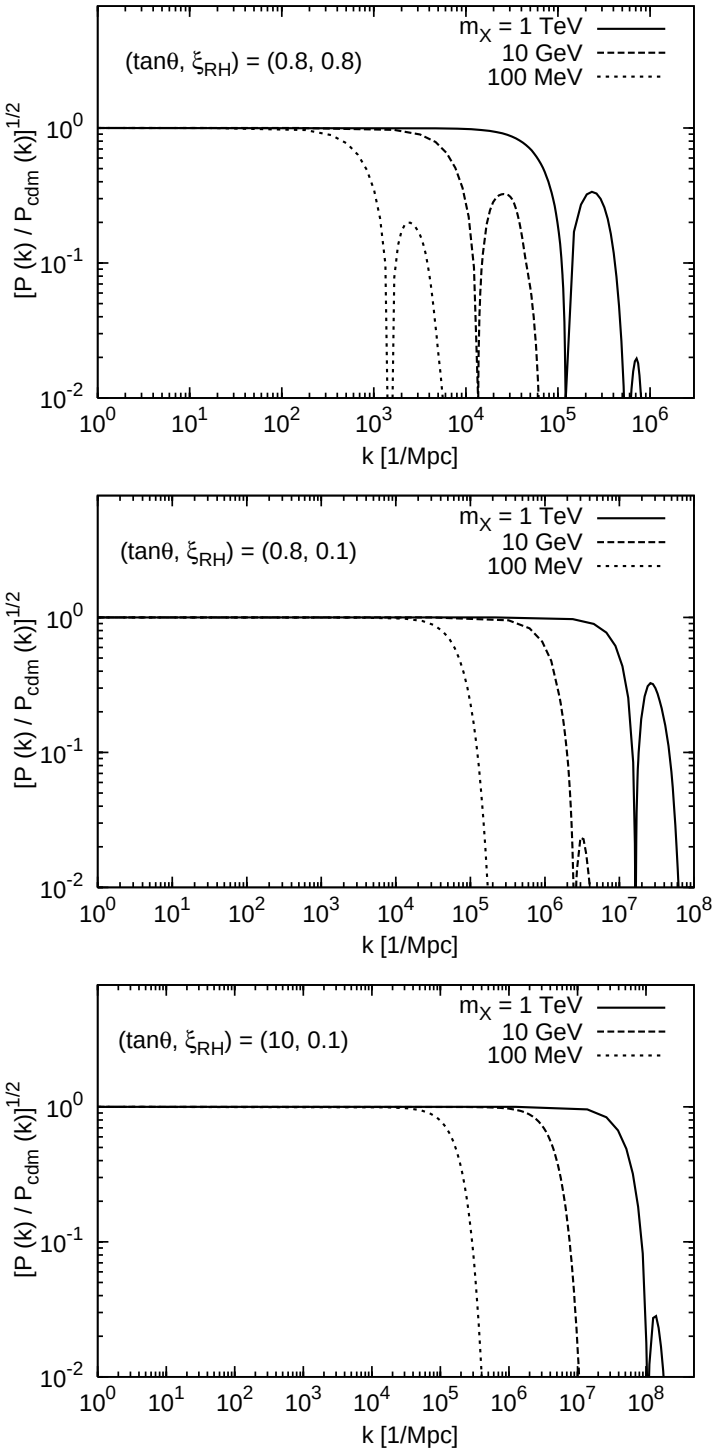

Figure 4. Transfer functions of the normalized dark matter density perturbation amplitude for $(\tan\theta_W^h, \xi_{\rm RH}) = (\sqrt{3/5}, 0.8)$ (top), $(\sqrt{3/5}, 0.1)$ (middle), and $(10, 0.1)$ (bottom).

JCAP07(2009)004

1 TeV, 10 GeV and 100 MeV, we find $k_{\rm cut} = 8.0 \times 10^4$ Mpc^{-1}, 9100 Mpc^{-1}, and 970 Mpc^{-1}, respectively. The free-streaming damping scale is

$$\lambda_{\rm fs} \approx \left[\Gamma\left(\frac{1}{2}\right)\frac{T^h_{\rm kd}}{m_X}\right]^{\frac{1}{2}} \eta_d \ln\left(\frac{\eta_{\rm eq}}{\eta_d}\right) , \tag{4.1}$$

where η_d is the comoving horizon at the time of kinetic decoupling, and $\eta_{\rm eq}$ is the comoving horizon at matter-radiation equality, and $\Gamma(1/2) = \sqrt{\pi}$. For $m_X = 1$ TeV, 10 GeV, and 100 MeV, we find $\lambda_{\rm fs}^{-1} = 9.3\times10^5$ Mpc^{-1}, 3.8×10^4 Mpc^{-1}, and 1500 Mpc^{-1}, respectively. We see that for these masses, $\lambda_{\rm fs} < k_{\rm cut}^{-1}$ — the cut-off scale is determined by the acoustic damping.

In figure 4, we also show the transfer function of the dark matter density perturbation for the cases $(\tan\theta^h_W, \xi_{\rm RH}) = (\sqrt{3/5}, 0.1)$ (middle panel), and $(10, 0.1)$ (bottom panel). Comparing with the top panel, we can see the transfer function cuts off at larger wavenumber for colder hidden sectors. Kinetic decoupling happens earlier and only the small scale modes that entered the horizon before kinetic decoupling get suppressed. For $m_X = 1$ TeV, the cut-off is determined by the acoustic damping scale. However, for $m_X = 10$ GeV and 100 MeV, the free-streaming damping scale is comparable to the acoustic damping scale.

The matter power spectrum contains all the information about linear Gaussian density fluctuations. These fluctuations are amplified by gravity to create non-linear structures, that is, dark matter halos. However, on scales below the cut-off the matter distribution is smooth and gravity cannot regenerate power on these scales. Thus the linear power spectrum also encodes information about the smallest building blocks of dark matter halos. The minimal mass of dark matter clumps may be estimated as

$$M_{\rm cut} = \frac{4\pi}{3}\left(\frac{\pi}{k_{\rm cut}}\right)^3 \Omega_m \rho_{\rm crit} , \tag{4.2}$$

where Ω_m is the matter density today, and $\rho_{\rm crit} = 3H_0^2/(8\pi G) = 8.1h^2 \times 10^{-47}$ GeV^4 is the present critical density.

In figure 5 we show the characteristic mass of the smallest objects as a function of dark matter mass m_X for various values of $(\tan\theta^h_W, \xi_{\rm RH})$. For the lower reheating temperature parameter $\xi_{\rm RH}$, $M_{\rm cut}$ is smaller by a few orders of magnitude for a given dark matter mass. For cold hidden sectors, kinetic decoupling occurs earlier, corresponding to smaller comoving horizons and larger $k_{\rm cut}$, which leads to smaller $M_{\rm cut}$. We can understand this more quantitatively. The parameter $k_{\rm cut}$ is related to the comoving horizon when kinetic decoupling happens as $k_{\rm cut}\eta_d = x_d$, where a typical value is $x_d \sim 5.9$ in our case. On the other hand, we have $\eta_d \sim 1/T_{\rm kd}$, so $k_{\rm cut}$ is proportional to the decoupling temperature, that is, $k_{\rm cut} \sim T_{\rm kd}$, and therefore $M_{\rm cut} \sim (T_{\rm kd})^{-3}$. As an example, consider the $m_X = 1$ TeV case. From figure 2, the ratio of visible decoupling temperatures for the $(\tan\theta^h_W, \xi_{\rm RH}) = (\sqrt{3/5}, 0.8)$ and $(\sqrt{3/5}, 0.1)$ cases is 7×10^{-3}, and so the expected ratio of minimum halo masses is 3×10^6 as may be ascertained from figure 5.

Our results in figure 5 show that the minimum halo mass — the building blocks of structure in the universe — could range anywhere from $10^{-10} M_\odot$ to the size of the smallest galaxies observed in the universe for dark matter masses within the MeV to TeV range. We will see in section 7 that if we restrict our attention to $\tan\theta^h_W < 10$, we will require $m_X \gtrsim 1$ GeV to obtain the right relic density and be consistent with the observed morphology of galactic dark matter halos. For this range of parameter space, we see from figure 5 that the minimum mass halos are less than about $10^4 M_\odot$. At the present time, there is no

JCAP07(2009)004

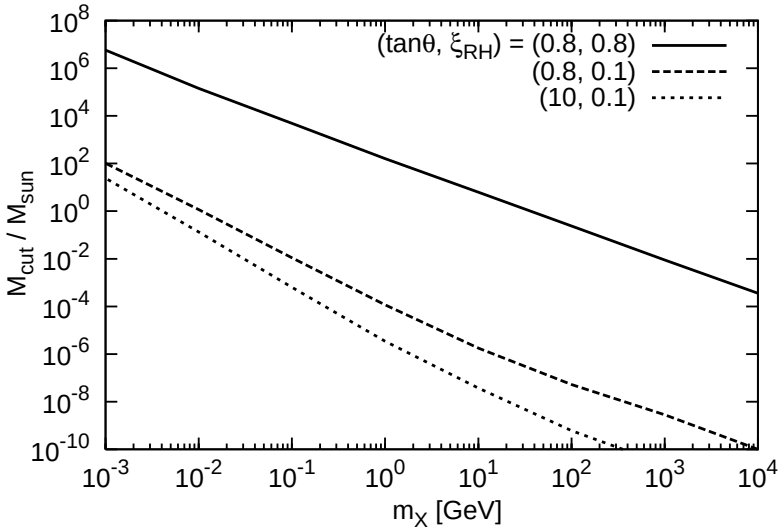

Figure 5. Mass of the smallest virialized dark matter structure that can form, as a function of the dark matter mass m_X for $(\tan\theta_W^h, \xi_{\rm RH}) = (\sqrt{3/5}, 0.8), (\sqrt{3/5}, 0.1), (10, 0.1)$, as indicated.

way to test for halo masses as small as this. These predictions for structure formation are therefore indistinguishable from those of WIMP models, and current observations do not place constraints on the hidden charged dark matter parameter space.

In the future, it may become possible to probe the upper end of this range with strong gravitational lensing of radio-loud quasars [61]. In addition, if the dark sector is linked to the visible sector through connector particles with both visible and hidden sector quantum numbers [12–14], then self-annihilations of dark matter within these mini-halos might provide a detectable signature for the Fermi gamma-ray experiment [62–69].

5 Bound state formation and Sommerfeld-enhanced annihilations in the early universe

Charged dark matter annihilation may be enhanced in two ways. First, at low velocities, its annihilation cross section is enhanced by the Sommerfeld effect [28]; in Feynman diagrammatic language, this enhancement arises from diagrams with additional $\mathrm{U}(1)_{\rm EM}$ gauge bosons exchanged in the t-channel that are higher order in gauge coupling, but kinematically enhanced at low velocities [70–72]. Second, charged dark matter may form bound states, which then annihilate. These are independent effects that must be included separately. Both act to enhance annihilation, and one might worry that they have negative implications. For example, the resulting enhanced annihilation rates may reduce the thermal relic density after chemical freeze out to negligible levels or otherwise change the relic density in a way that is excluded by astrophysical observations.

In full generality, these effects may be evaluated by solving the coupled Boltzmann equations for the number densities of the bound state $B \equiv (\tilde{\tau}^{h+}\tilde{\tau}^{h-})$ and the dark matter

JCAP07(2009)004

particle $X \equiv \tilde{\tau}^h$,

$$\begin{aligned}\frac{dn_B}{dt} + 3Hn_B &= n_X\Gamma_{\rm rec} - n_B\Gamma_B - n_B\Gamma_{\rm ion}\\ \frac{dn_X}{dt} + 3Hn_X &= -n_X\Gamma_{\rm ann} - n_X\Gamma_{\rm rec} + n_B\Gamma_{\rm ion}\,,\end{aligned} \tag{5.1}$$

where

$$\begin{aligned}\Gamma_{\rm rec} &\equiv \Gamma(X^+X^- \to B\gamma^h) = C\,n_X\,\langle\sigma_{\rm rec}v\rangle\\ \Gamma_B &\equiv \Gamma(B \to \gamma^h\gamma^h) = \frac{\alpha_X^5\,m_X}{2}\\ \Gamma_{\rm ion} &\equiv \Gamma(B\gamma^h \to X^+X^-) = n_{\gamma^h}\,\langle\sigma_{\rm ion}v\rangle\\ \Gamma_{\rm ann} &\equiv \Gamma(X^+X^- \to \gamma^h\gamma^h) = C\,n_X\,S\,\langle\sigma_A v\rangle\,,\end{aligned} \tag{5.2}$$

are the recombination (bound state formation) rate, the bound state decay width, the ionization rate, and the Sommerfeld-enhanced dark matter annihilation rate, respectively. In eq. (5.2), $C = \langle\rho^2\rangle/\langle\rho\rangle^2$ accounts for the clumping of dark matter into halos, σ_A is the tree-level S-wave annihilation cross section, and

$$S = \frac{\pi\alpha_X/v}{1 - e^{-\pi\alpha_X/v}} \tag{5.3}$$

is the Sommerfeld enhancement factor [28, 73], where v is the center-of-mass velocity of the incoming particles. For $v \gtrsim \alpha_X$, $S \sim 1$, but for $v \ll \alpha_X$, $S \sim \pi\alpha_X/v$ may be a significant enhancement. The recombination and photoionization and cross sections are related through the Milne relation

$$\frac{\sigma_{\rm ion}}{\sigma_{\rm rec}} = \left(\frac{m_X\,v}{B_n + \frac{1}{2}m_X\,v^2}\right)^2 \frac{g_{\tilde{\tau}}^2}{2\,g_n}\,, \tag{5.4}$$

where $g_{\tilde{\tau}} = 1$ and $g_n = 1$ are the statistical weights of the staus and the n-th level of the bound state, and $B_n = \alpha_X^2\,m_X/4n^2$ is the binding energy of bound state level n. Photoionization may, in principle destroy bound states before they annihilate.

The recombination rate requires some analysis. First, note that a photon is radiated in the recombination process; bound state formation followed by bound state decay yields a different final state than Sommerfeld-enhanced annihilation, and these two effects must be included separately; as we will see, both yield an enhancement that is parametrically $\sim \alpha_X/v$ for small velocities.

The recombination cross section may be determined by using a hydrogen atom wavefunction solution in the Schrödinger equation for a particle moving in a central potential $V(r) \sim -\alpha_X/r$. The recombination cross section for the n-th shell is [74]

$$\sigma_{\rm rec}^{(n)} = \frac{2^8\pi^2}{3}\,\frac{\alpha_X}{m_X}\,\frac{1}{m_X}\,\frac{B_n}{m_X v^2}\left(\frac{B_n}{B_n + \frac{1}{2}m_X v^2}\right)^2 \cdot \frac{e^{-4\sqrt{\frac{2B_n}{m_X v^2}}\,\tan^{-1}\sqrt{\frac{m_X v^2}{2B_n}}}}{1 - e^{-2\pi\sqrt{\frac{2B_n}{m_X v^2}}}}\,. \tag{5.5}$$

This result includes a correction factor from the fact that the electromagnetic force is long range, so that the incoming state is not a plane wave. The phase space distribution of the $\tilde{\tau}^h$ cold dark matter is given by solving the Boltzmann equation of eq. (3.1). The solution is

JCAP07(2009)004

a Boltzmann distribution with dark matter temperature $T_X \sim T^h$ before kinetic decoupling, and an effective temperature

$$T_X \to \frac{T^{h\,2}}{m_X}\,\frac{m_X}{T^h_{\rm kd}} \tag{5.6}$$

after kinetic decoupling. The $\tilde{\tau}^h$ thus has Maxwellian velocity distribution at the effective temperature T_X,

$$f(v)\,dv = 4\pi\left(\frac{m_X}{2\pi T_X}\right)^{3/2} v^2\, e^{-\frac{m_X v^2}{2T_X}}\,dv\ . \tag{5.7}$$

Summing over all binding states, the thermally averaged total recombination cross section is

$$\begin{aligned}\langle\sigma_{\rm rec} v\rangle \ &= \ \sum_n \int dv f(v)\,\sigma^{(n)}_{\rm rec}\,v \\ &= \sum_n \frac{4}{\sqrt{\pi}}\,\frac{2^8\pi^2}{3}\,\frac{1}{v_0^3}\,\frac{\alpha_X}{m_X^3}\,B_n \int dv\, v\,\frac{B_n^2\, e^{-v^2/v_0^2}}{(B_n+\frac{1}{2}m_X v^2)^2}\,\frac{e^{-4\sqrt{\frac{2B_n}{m_X v^2}}\,\tan^{-1}\sqrt{\frac{m_X v^2}{2B_n}}}}{1-e^{-2\pi\sqrt{\frac{2B_n}{m_X v^2}}}} \\ &\to \frac{(4\pi\,\alpha_X)^2}{m_X^2}\,\frac{1}{8\pi}\,\frac{\pi\alpha_X}{v_0}\left(\frac{2^6\,e^{-4}}{3\sqrt{\pi}}\right)\left(\sum_n \frac{1}{n^2}\right), \qquad \frac{v_0}{\alpha_X} \ll \frac{1}{n}\,,\end{aligned} \tag{5.8}$$

where we have made the replacement $v_0^2 = 2\,T_X/m_X$. We see that in the small kinetic energy limit, the thermally averaged recombination cross section is the thermally averaged annihilation cross section of eqs. (2.3) and (2.4), enhanced by a "bound state enhancement factor," that is, $\langle\sigma_{\rm rec} v\rangle = S_{\rm rec}\,\langle\sigma_A v\rangle$, with

$$S_{\rm rec} \sim 0.7\left(\frac{1}{8\pi\,a_0}\right)\left(\frac{\alpha_X}{v_0}\right), \qquad v_0/\alpha_X \ll 1\ . \tag{5.9}$$

The numerical prefactor is, for example, 0.5 and 0.05 for $\tan\theta^h_W = \sqrt{3/5}$ and 10, respectively. Summing to higher binding states would give a factor of $\simeq 1.6$ at most.

In figure 6 we plot the bound state formation rates $\Gamma_{\rm rec}$ for $m_X = 1$ GeV and 1 TeV. After chemical freeze out and before the bound state formation can take place, the cold dark matter number density is $n_X = \Omega_X\,\rho_{\rm crit}\,a^{-3}/m_X \propto T^3$. Here we compare in the era before matter-radiation equality where the dark matter particles have not clumped into halos yet. Next we will consider enhanced annihilation and bound state formation in the earliest bound objects, the protohalos. The bound state formation rate for different dark matter masses m_X may be understood as follows. In general, there are three stages:

1. Before kinetic decoupling the dark matter most probable speed is $v_0 \propto T^{1/2}$. When $v_0/\alpha_X \gg 1$ the thermally averaged bound state formation cross section goes as $\langle\sigma_{\rm rec} v\rangle \propto 1/v_0^3$ and hence the rate $\Gamma_{\rm rec} \propto T^{3/2}$.

2. After kinetic decoupling, the dark matter most probable speed becomes $v_0 \propto T$. When $v_0/\alpha_X \gg 1$ still holds, the bound state formation rate is $\Gamma_{\rm rec} \propto T^3\,v_0^{-3} =$ constant.

3. When the dark matter velocity drops to the point $v_0/\alpha_X \lesssim 1$, $\langle\sigma_{\rm rec} v\rangle$ becomes $\propto 1/v_0$ (cf. eq. (5.8)). As a consequence $\Gamma_{\rm rec}$ decreases as T^2, the same as the Hubble rate in the radiation-domination era.

JCAP07(2009)004

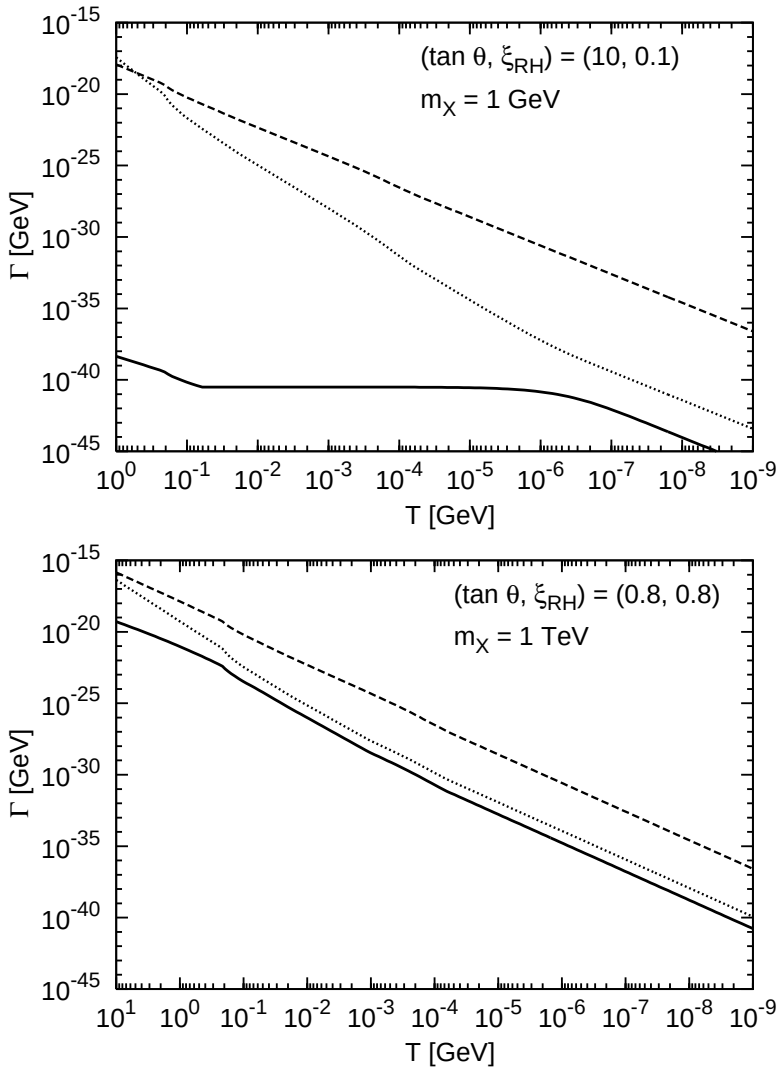

Figure 6. The recombination rates (bound state formation rates) $\Gamma_{\rm rec}$ (solid) in the early universe as functions of the visible (CMB) temperature for dark matter mass $m_X = 1$ GeV and $(\tan\theta_W^h, \xi_{\rm RH}) = (10, 0.1)$ (upper) and $m_X = 1$ TeV and $(\tan\theta_W^h, \xi_{\rm RH}) = (\sqrt{3/5}, 0.8)$ (lower). Also shown are the Sommerfeld-enhanced annihilation rates $\Gamma_{\rm ann}$ (dotted) and the Hubble expansion rate H (dashed).

Also shown in figure 6 are the Hubble expansion rate H and the Sommerfeld-enhanced annihilation rates $\Gamma_{\rm ann}$. The results can be summarized as

$$H \gg \Gamma_{\rm ann} \gtrsim \Gamma_{\rm rec} \tag{5.10}$$

for $m_X = 1$ GeV $-$ 10 TeV. The bound state decay rate Γ_B and photoionization rate $\Gamma_{\rm ion}$ can be much larger than the Hubble rate. But since bound states rarely form, we may set $n_B = 0$ in eq. (5.1). We see that for $v \ll \alpha_X$, bound state formation has qualitatively the same effect on annihilation as the Sommerfeld effect — they enhance annihilation by factors of S and $S_{\rm rec}$, which are both proportional to α_X/v, with order one coefficients. Since the Sommerfeld enhancement factor is also valid for $v \gtrsim \alpha_X$, while the bound state effect becomes

JCAP07(2009)004

negligible at large v, one may draw qualitatively correct conclusions by considering only the Sommerfeld effect and neglecting the effects of bound state formation, but we emphasize that these effects are independent, yielding two different final states.

We may now answer the questions posed at the beginning of this section. Because the Hubble expansion rate is larger than the Sommerfeld-enhanced and bound state-catalyzed annihilation rates, the thermal relic density is not modified significantly between the times of chemical freeze out and matter-radiation equality.

6 Sommerfeld-enhanced annihilations in protohalos

We now consider these non-perturbative effects on the dark matter annihilation after matter-radiation equality, when the growth of structure enters the non-linear regime. The smallest structures undergo gravitational collapse first and the more massive ones form later. The minimum halo mass $M_{\rm cut}$ is set by the cold dark matter kinetic decoupling temperature and we have computed this for the hidden charged dark matter in section 4 (cf. figure 5). The redshift at which these objects form (virialize) depends on the underlying matter power spectrum [75], which we have also computed in section 4. Simulations [76] find $z_c \sim 30$ for a typical $10^{-6}\,M_\odot$ halo and we will assume this value in this work, but note that in detail the collapse redshift depends on $M_{\rm cut}$. We take the overdensity of the virialized region to be $\simeq 178$ times the ambient cosmological density at z_c (appropriate for WMAP cosmology) and estimate the velocity dispersion of the dark matter particles in the halo as:

$$v_0 = \sqrt{\frac{G M_{\rm cut}}{R_{\rm vir}}} \simeq 3.0 \times 10^{-8} \left(\frac{M_{\rm cut}}{M_\odot}\right)^{1/3} (1+z_c)^{1/2} \,. \tag{6.1}$$

Hidden charged dark matter particles in our model with masses $m_X \gtrsim 1$ GeV have velocity dispersion $v_0 \ll \alpha_X$ in these protohalos. They thus form bound states and pair-annihilate with an enhanced cross section, from an initial number density $n_X \simeq 6\,(m_X/{\rm GeV})^{-1}\,{\rm cm}^{-3}$ for about a Hubble time before the protohalos merge into larger halos. In these larger halos, the dark matter particles have smaller phase space density and so the annihilation rate is lower.

Dark matter annihilation in protohalos was used in ref. [32] to obtain stringent constraints on models with the Sommerfeld enhancement effect. In that work dark matter particles were assumed to annihilate dominantly to visible photons and e^+e^- pairs, which contribute to the extragalactic diffuse gamma-ray flux and generate CMB temperature and polarization power spectra. However, in the present context, where the hidden sector is not coupled to the visible sector, only a much weaker, separate, constraint from CMB anisotropy measurements applies. The CMB measurement of the matter density $\Omega_m h^2$ can be compared with those obtained by distance measurements using Supernovae Type Ia (SNIa) and baryon acoustic oscillations (see, for example, ref. [77]). A rough estimate will suffice for our purposes here and we will assume that no more than 10% of the total matter can be converted into radiation between the epoch of recombination and now.

This constraint may then be applied to our models, where the S-wave stau annihilation cross section of eq. (2.3) is enhanced by the Sommerfeld factor S. As mentioned before, when $v_0/\alpha_X \ll 1$ the bound state formation cross section is of comparable size. One demands the fraction of stau annihilation in the protohalos

$$f \simeq n_X\, S\, \langle \sigma_A\, v \rangle\, C\, t \simeq \frac{178\,\Omega_c\,\rho_{\rm crit}\,(1+z_c)^3}{m_X}\, S\, \langle \sigma_A\, v \rangle\, C\, t \,\leq\, 0.1\,, \tag{6.2}$$

JCAP07(2009)004

during $t \simeq 5.6 \times 10^{17}\,(1+z_c)^{-1.5}$ s, the age of the universe at redshift $z_c \gg 1$. The density profile of the minimum mass halos [76] is expected to be similar to those of the larger halos [75], and we include an appropriate clumping factor $C = 7$ for the minimum halo mass. We find that for $(\tan\theta_W^h, \xi_{\rm RH}) = (10, 0.1)$, $f \sim 10^{-8} - 10^{-5}$ for $m_X = 1$ GeV $-$ 10 TeV and α_X fixed by $\Omega_X h^2 = 0.11$. For $(\tan\theta_W^h, \xi_{\rm RH}) = (\sqrt{3/5}, 0.8)$ and $(\sqrt{3/5}, 0.1)$, $f \sim 10^{-7} - 10^{-5}$ for the same mass range and the corresponding α_X's. These values are far below the bound of $f \leq 0.1$, and so the annihilation of dark matter in protohalos does not constrain the scenario in the case of purely hidden charged dark matter. However, if there were connector particles with both hidden and visible sector quantum numbers mediating annihilation to observable particles, a much more stringent bound $f \lesssim 10^{-9}$ may apply [32]. This is from the consideration that (visible) photons ejected at an energy $\gtrsim 300$ GeV or $\lesssim 100$ keV should not lead to heating and ionization of the intergalactic medium that contradicts CMB and large scale structure observational data.

More massive halos have larger dark matter velocity dispersions. For example, Milky Way-size halos have $v_0 \sim 270$ km/s $\sim 10^{-3}$, while dwarf galaxies can have velocities as low as $v_0 \sim 10$ km/s $\sim 7 \times 10^{-5}$. For hidden charged dark matter particles with masses $m_X =$ 1 GeV $-$ 10 TeV, then, only a fraction $f \sim 10^{-7}$ annihilates during the age of the Universe.

7 Ellipticity and cores of dark matter halos

At late times, elastic scattering between $\tilde{\tau}^h$ dark matter particles in the halos of galaxies or clusters of galaxies may change the shape of constant-density contours and lead to the formation of a core, that is, a central region with constant density. The main effect results from transfer of kinetic energy in collisions and if this process is fast enough to create $\mathcal{O}(1)$ changes to the energy of the dark matter particles in the halo, then it will drive the halo towards isothermality and isotropize the mass distribution.

The true dynamical picture is more complicated. Initially, heat is conducted from the hotter outer to the cooler inner parts of the halo through collisions. This heats up the core causing it to puff up, which gives rise to a density profile that is much shallower (or even flat) compared to the initial cuspy density profile of the central regions of the halo. In addition, self-annihilations will also lead to cores [78], however our calculation in section 6 has shown that this is a not large effect. The collisions also erase velocity correlations and lead to more a more spherical (rounder) core. We find that the observed ellipticity of galactic dark matter halos provides the strongest constraints on charged dark matter models.

Over periods long compared to the relaxation time, ejection of dark matter particles from the parent halo in collisions will further cool the core. For an isolated halo, this will eventually lead to core collapse and result in a steep cusp. In a cosmological setting, however, halos accrete dark matter particles and this would offset the energy loss due to collisions. Cosmological simulations [79, 80] seem to indicate that core collapse occurs on a time scale much longer than the relaxation time scale, if at all. We will, therefore, not consider this effect any further here.

Shapes of dark matter halos of elliptical galaxies [81, 82] and clusters [34, 83] are decidedly elliptical and this fact may be used to put constraints on the self-interactions. Such an analysis [34] was carried out in the context of the self-interacting dark matter proposal [84]. This proposal was designed to explain why observations of the rotation curve of low surface brightness galaxies seemed to indicate that the dark matter distribution had a flat density profile in the inner core [85–87] and to explain the observed census of dwarf galaxies in the

JCAP07(2009)004

Local Group [88, 89]. The status of these discrepancies is unclear — while it seems clear that the census of the observed local group galaxies are broadly in agreement with the cold dark matter model [90, 91], the fit to rotation curves of low-surface brightness galaxies is still problematic [92–96].

The strongly self-interacting dark matter proposal motivated the first numerical simulations to deduce the effects of dark matter self-interaction [33, 79, 97–103] and they validated the expectation that during the evolution to isothermality, the dark matter core becomes rounder. These simulations indicated that only regions of parameters space with $500\ \mathrm{GeV}^{-3} \lesssim \sigma_{\rm DM}/m_X \lesssim 5000\ \mathrm{GeV}^{-3}$ ($0.1\ \mathrm{cm}^2/\mathrm{g} \lesssim \sigma_{\rm DM}/m_X \lesssim 1\ \mathrm{cm}^2/\mathrm{g}$) could introduce observable features on the scale of the dwarf galaxies while at the same time being consistent with observations of larger galaxies. In the constraint quoted above, $\sigma_{\rm DM}$ is the dark matter elastic self-scattering cross-section modeled as a hard-sphere interaction. The analysis of the shape of the dark matter halo of a particular cluster of galaxies (using gravitational lensing) indicated that much of the above preferred region was ruled out [34].

We revisit the constraint from the inferred ellipticity of dark matter halos in the rest of this section. These constraints arise from a wide-range of observations including X-rays [81, 83], strong lensing [104–106] and weak lensing [107–109]. Recent work on combining different measurements to reveal the anisotropy of velocity dispersion [110] in clusters (as opposed to the shape of dark matter distribution) is a different but complementary way to constrain the self-interaction of dark matter.

To estimate how these observations may be used to constrain the dark sector Coulomb interactions, we calculate the relaxation time for establishing an isothermal halo. We will then assume that the time scale for isotropizing the spatial distribution of the dark matter halo is the same as this relaxation time and use constraints from measurements of the ellipticity of galaxy halos to put limits on the dark sector Coulomb interaction. The notable feature of the Coulomb interaction is the strong dependence of the energy transfer rate on the relative velocity of the interacting particles. This ties in with other investigations that considered velocity-dependent interaction cross sections. See, for example, refs. [111–116].

The Rutherford scattering cross section is

$$\frac{d\sigma}{d\Omega} = \frac{\alpha_X^2}{4m_X^2 v^4 \sin^4(\theta/2)}\,, \tag{7.1}$$

where θ is the scattering angle in the lab frame. We assume the dark matter particles in the halos have a local Maxwellian velocity distribution $f(v)$ (normalized to unity) and velocity dispersion $\langle v^2\rangle = (3/2)v_0^2(r)$, which in general varies spatially within a halo. The kinetic energy exchange in each collision is $\delta E_k = E_k\,(1-\cos\theta)$, where $E_k = m_X v^2/2$. The rate of energy transfer is, then,

$$\begin{aligned}
\dot{E}_k &= \int dv\, d\Omega \frac{d\sigma}{d\Omega} f(v)\, \delta E_k\, v\, n_X \\
&= 2\pi\, \frac{\alpha_X^2}{4m_X^2}\, \frac{4}{\sqrt{\pi}}\, \frac{1}{v_0^3}\, \frac{1}{2} m_X\, \frac{\rho_X}{m_X} \int dv\, d\cos\theta \frac{1-\cos\theta}{\sin^4(\theta/2)}\, v\, e^{-v^2/v_0^2} \\
&= -\frac{2\alpha_X^2 \rho_X \sqrt{\pi}}{m_X^2\, v_0^3} \ln(1-\cos\theta_{\rm min})\, v_0^2\,.
\end{aligned} \tag{7.2}$$

The minimum scattering angle is related to the maximum impact parameter through

$$b_{\rm max} = \frac{\alpha_X}{m_X v_0^2} \cot(\theta_{\rm min}/2)\,, \tag{7.3}$$

JCAP07(2009)004

where $b_{\rm max}$ should be chosen to be

$$\lambda_D \sim \frac{m_X\, v_0}{\sqrt{4\pi\, \alpha_X\, \rho_X}}\,, \tag{7.4}$$

the Debye screening length in the $\tilde{\tau}^h$ plasma. We find constraints on α_X by demanding that the relaxation time be larger than the age of the universe,

$$\tau_{\rm r} \equiv E_k/\dot{E}_k \simeq \frac{m_X^3\, v_0^3}{4\sqrt{\pi}\, \alpha_X^2\, \rho_X} \left(\ln \left(\frac{\left(b_{\rm max}\, m_\chi v_0^2 \alpha_X^{-1}\right)^2 + 1}{2} \right) \right)^{-1} \geq 10^{10}\ \text{years}\,, \tag{7.5}$$

where the "Coulomb logarithm" is ~ 90. The constraints on α_X obtained above scale inversely with the square root of the "phase space density" $Q \equiv \rho_X/v_0^3$, and this indicates that the best constraints may be obtained by studying the cores of galaxies rather than clusters of galaxies.

Many elliptical galaxies show clear evidence for flattened, triaxial dark matter halos [81]. Using the profiles of the total mass enclosed $M(r)$ and the halo concentration parameters c from refs. [117, 118], we derive the radial velocity dispersion $\overline{v_r^2}(r) = (3/2)v_0^2(r)$ and the dark matter density $\rho_X(r)$ at a radius $\sim 3 - 10$ kpc. The dark matter density drops from 3.5 to $0.7\,\text{GeV/cm}^3$ as one moves outwards, while the velocity dispersion decreases slightly from 270 to 250 km/s. Using these values in eq. (7.5), we obtain a very stringent bound on α_X. This constraint is shown as the lower solid line in figure 1. If we demand that the WIMPless scenario provide the right relic abundance of $\Omega_X h^2 \simeq 0.11$, then for $(\tan\theta_W^h, \xi_{\rm RH}) = (\sqrt{3/5}, 0.8)$ and $(\sqrt{3/5}, 0.1)$, $m_X \gtrsim 100$ GeV. However, for $(\tan\theta_W^h, \xi_{\rm RH}) = (10, 0.1)$, hidden charged dark matter as light as $m_X \sim 1$ GeV may freeze out with the correct thermal relic density without being in conflict with the constraint from elliptical halos.

The constraints obtained above are comparable to those deduced in ref. [19]. This previous work demanded that the properties of the Milky Way's dark matter halo (and by extension that of other galaxies as massive as the Milky Way) should not deviate by order unity from those predicted by collisionless dark matter simulations. If we compare their result to our eq. (7.5) with $\rho_X = 0.3$ GeV cm^{-3} and $v_0 = 200$ km s^{-1}, we obtain weaker constraints on α_X by a factor of ~ 6 at the same m_X. We trace the bulk of this discrepancy to the fact that they assume total dark matter mass of $10^{10} M_\odot$ in their calculation and neglect the contribution of stars in setting the local dark matter velocity dispersion. The constraints we have obtained from detailed observations of an elliptical galaxy with strong X-ray emission resolved down to 3 kpc of the center — better than we can do within our own galaxy for now — are comparable to the bounds quoted in ref. [19]. Future observations of hyper-velocity stars within the Milky Way could strengthen these constraints [119].

We may also consider dark matter halos more massive and less massive than that of the Milky Way. Cluster halo shapes are measured with X-rays and strong gravitational lensing at radii ~ 100 kpc. We consider some Abell clusters for which the ellipticity profiles are determined in ref. [83]. The radial velocity dispersion at this scale is typically $\sqrt{\langle v_r^2 \rangle} \sim 1000$ km/s, as inferred from the $M(r)$ profiles determined in ref. [120]. As a consequence the bounds on α_X are about two orders of magnitude weaker.

In principle, the most stringent constraint using eq. (7.5) would be from smaller spiral galaxies and the Local Group dwarf galaxies, where we expect larger dark matter phase space densities and therefore shorter relaxation times. Current observations of the shapes of dark matter halos of nearby spiral galaxies [121] find, however, that their gravitational potential is

JCAP07(2009)004

quite round, and that they seem to prefer a central core. It is interesting to note that within our model, the effect of dark sector Coulomb interactions could leave a dynamical imprint in some of these nearby spiral galaxies but not the larger elliptical galaxies. We leave more detailed investigations for future work.

The case of the dwarf galaxies in the Local Group, that is, the satellites of the Milky Way and Andromeda galaxies, is particularly interesting. The stars in these galaxies have very small velocity dispersions — of the order of 10 km/s or even smaller. Combining this with the observed extent of the stellar population, one may infer the mass of the dark matter within the stellar extent of these dwarf galaxies. The results of such an analysis show that the dwarf satellites of the Milky Way are consistent with dark matter central densities of about $0.1 M_\odot/\mathrm{pc}^3 \simeq 4$ GeV/cm^3 [122]. Unlike the galaxies we have been considering previously, these dwarfs present a complication. Their present day properties are set rather dramatically by the Milky Way galaxy. As they fall into the Milky Way, gravitational tidal forces will strip them of mass on the outside and thus reduce the velocity dispersion of the dark matter particles inside the satellite's halo. Exactly what the dispersion is depends on the initial mass, the extent of the tidal mass loss and dark matter self-interactions. If the dispersion is of the order of 10 km/s (similar to the observed stellar velocity dispersion), the energy transfer time scale is short in the dwarf satellites for α_X and m_X that are at the edge of the allowed region in figure 1. For these values of m_X and α_X, interactions will almost certainly form cores in the dwarf galaxies. Such cores are compatible with observations unless they are larger than about 300 pc [123, 124]. Future astrometric measurements of individual stars in these satellite galaxies will be able to measure the density profile of dark matter halos on these scales [125].

Surprisingly, if we use the relation between the core radius and core density for a self-gravitating isothermal sphere, $\rho_{\mathrm{core}} = 9v_0^2/(4\pi G r_{\mathrm{core}}^2)$ with $v_0 = 10$ km/s and $\rho_{\mathrm{core}} \simeq 4$ GeV/cm^3 [122], we obtain a core size of 200 pc. However, our estimate has not accounted for some crucial factors. If the mean free path is much shorter than the typical orbit of the dark matter particles within the satellite, heat conduction will be suppressed. In addition, the passage through the Milky Way will introduce interactions with the dark matter in the Milky Way and this could change the density profile of the satellite.

More detailed work is required to consider the effect of dark sector Coulomb interactions on the satellites of the Milky Way and other galaxies. We conjecture here that there would be regions of allowed parameter space where the satellites galaxies and other small field galaxies would show constant density cores in the center and reduced substructure within their halos. This is beyond the scope of the present work, but we urge the reader to keep in mind that future work in this direction could lead to interesting astrophysical phenomena and perhaps also rule out some of the allowed parameter space.

8 Dark matter in the bullet cluster

The Bullet Cluster is a rare system where a subcluster is seen to be moving through a larger cluster. Through observations in the optical and X-ray and strong and weak gravitational lensing observations, astronomers have been able to map out the spatial distributions of the stars, gas and dark matter in this system. From these inferred distributions, it is clear that dark matter tracks the behavior of stars, which are collisionless, rather than the gas. This observation has allowed stringent bounds to be placed on the dark matter self-interaction strength.

JCAP07(2009)004

With respect to the self-interacting dark matter proposal [84] discussed in the previous section (velocity-independent cross section), the Bullet Cluster observations demand [33, 126] that $\sigma_{\rm DM}/m_X \lesssim 3000\ {\rm GeV}^{-3}$ ($\sigma_{\rm DM}/m_X \lesssim 0.7\ {\rm cm}^2/{\rm g}$). These are the most direct constraints on the self-interaction of dark matter.

These bounds have been derived based on different considerations, including the observed gas and dark matter offset, the high measured subcluster velocity, and the survival of the subcluster after having moved through the Bullet Cluster [126]. The last phenomenon, survival of the subcluster, turns out to provide the strongest constraint and hence we will focus on that. We follow the approach of ref. [126] to derive bounds on the dark sector Coulomb interaction, but relax the assumption of a hard-sphere interaction cross section.

The subcluster experiences a net particle loss in a collision when the velocities of both particles in the main and subcluster become larger than the escape velocity $v_{\rm esc} \simeq 1200$ km/s. This condition may be turned into an effective range for the scattering angle in the subcluster's reference frame

$$\frac{v_{\rm esc}}{v_1} < \cos\theta < \left(1 - \frac{v_{\rm esc}^2}{v_1^2}\right)^{1/2} , \tag{8.1}$$

where $v_1 \sim 4800$ km/s is the velocity of the main cluster incoming particle before the collision. We now assume that the subcluster passed through the main cluster's center so that it saw a surface density $\Sigma_m \sim 0.3\ {\rm g/cm}^2$. Demanding that the fraction of particle loss be no greater than 30%, we have an upper bound on α_X:

$$f \equiv \frac{\Sigma_m}{m_X} \int d\Omega\, \frac{d\sigma}{d\Omega} = \frac{\Sigma_m}{m_X}\, \frac{2\pi\, \alpha_X^2}{m_X^2\, v_1^4} \left[\frac{1}{1-\cos\theta_{\rm min}} - \frac{1}{1-\cos\theta_{\rm max}}\right] < 0.3\ . \tag{8.2}$$

This bound is given in figure 1. We see that it is about four orders of magnitude weaker than that obtained from considerations of the ellipticity of galactic dark matter halos. Equation (8.2) suggests that an improvement of this kind of bound can be made by considering a galaxy falling into a cluster, which results in a larger surface density $\Sigma_m = \int \rho_X dl \sim 30\ {\rm g/cm}^2$, where the galaxy path is $l \sim 2\pi R\, t_{\rm age}/6\tau_{\rm dyn}$. By demanding similarly that the galaxy does not lose more than 30% of its particles during orbiting in the cluster for about the age of the universe, we obtain a bound on α_X roughly ten times stronger than from the Bullet Cluster, but still weaker than the bounds obtained from the observed ellipticity of galactic dark matter halos in the previous section.

9 Conclusions

We have investigated the astrophysical and cosmological consequences of dark matter that is charged under an unbroken hidden $\mathrm{U}(1)_{\rm EM}$. We find that this is a viable and natural dark matter candidate. The salient arguments leading us to this conclusion are as follows.

- We investigated the dark matter-dark photon and dark matter-dark neutrino scattering processes in the early universe and found that the dark matter kinetically decouples early and therefore behaves as cold dark matter. The predictions for the temperature at which dark matter kinetically freezes out are shown in figure 2.

- Our calculations for the power spectrum of density fluctuations of dark matter showed that in these models (for $m_X >$ GeV) we expect structure all the way down to at least $10^4 M_\odot$. The predictions for these building blocks of structure in the Universe

JCAP07(2009)004

are summarized in figure 5. At the present time, we have no way to distinguish these hidden sector charged dark matter models from canonical WIMP models using matter power spectrum observations.

- Although the dark matter particles in our model are cold, they also have long-range Coulomb interactions (but with a smaller fine structure constant for masses below 1 TeV). Since the hidden sector $\mathrm{U}(1)_{\mathrm{EM}}$ is unbroken, we have equal numbers of positively and negatively charged particles and hence we investigated the formation of bound states. We found that for masses below 10 TeV, bound state formation and the subsequent annihilation does not change the relic density of dark matter particles appreciably.

- The self-interactions mediated by the long-range (hidden sector) Coulomb force can affect non-linear structure formation, especially at the small mass end. We found that the most stringent constraints arise from the observed ellipticity of galactic dark matter halos. (The self-interactions, if too strong, will make the core of dark matter halos round.)

- Putting together all of the results above, we find that the mass of a dark matter particle charged under a hidden sector unbroken $\mathrm{U}(1)_{\mathrm{EM}}$ must be larger than about a GeV, *if* we restrict our attention to hidden sector weak mixing angles $\tan\theta_W^h < 10$. Larger values of the weak mixing angle will allow smaller dark matter particle masses. The detailed constraints imposed by the galactic dark matter halo observations, the Bullet Cluster observations and the requirement of obtaining the right relic density are shown in figure 1.

- We also found that smaller galaxies such as the observed low surface brightness spirals and satellites of the Milky Way and Andromeda galaxy are likely to have constant density cores in their dark matter distribution. More work is required to pin down the core sizes, but this is clearly the regime where large differences from the predictions of collisionless cold dark matter, if any, will be found.

One of the promising avenues forward that we are currently exploring is including a connector sector linking the hidden and visible sectors. Such a connector sector will give rise to new phenomenology, further constraints [32, 127], and interesting implications for a variety of dark matter detection possibilities [13, 14, 17, 39].

A second promising avenue concerns structure formation on small scales. Our formalism suggests that in the allowed parameter space, the largest deviations from collisionless cold dark matter will appear in galaxies much less massive than the Milky Way. A detailed investigation of this aspect of hidden sector dark matter models is beyond the scope of the present work, but simple estimates suggest that, for large regions of model space, small galaxies will form cores and the substructure in all dark matter halos will be reduced. These expectations are in stark contrast to the predictions of collisionless cold dark matter models.

We also stress that there are many other possibilities in the hidden charged dark matter framework. We have considered the hidden stau as the dark matter. Other charged particles, for example, the hidden tau, chargino, quarks, and squarks, are also possible. This scenario also supports multi-component dark matter, with several hidden sectors, each with its own dark matter particle contributing significantly to the relic density through the WIMPless miracle. Alternatively, even with only one hidden sector, stable hidden staus and hidden (light, but massive) neutrinos could form mixed dark matter, with both hot and cold components. All of these scenarios merit further study.

JCAP07(2009)004

To summarize, we have investigated the astrophysics and cosmology of dark matter charged under a hidden unbroken $\mathrm{U}(1)_{\mathrm{EM}}$. We find that for dark matter masses larger than about a GeV, these models have the right relic density, make cosmological predictions currently indistinguishable from the usual WIMP models, and are consistent with observations on galactic and cluster scales. At the same time, these dark matter candidates are collisional and their annihilation is enhanced, implying consequences for future observations and experiments that may differ radically from WIMPs and other more conventional possibilities.

Acknowledgments

We thank Phil Humphrey, Jun Koda, Jason Kumar, and Quinn Minor for many helpful discussions. The work of JLF and HT was supported in part by NSF grant PHY–0653656. The work of MK was supported in part by NSF grant PHY–0555689 and NASA grant NNX09AD09G. The work of HY was supported in part by NSF grants PHY–0653656 and PHY–0709742.

A Calculation of dark matter power spectrum

In this appendix, we outline the calculation to compute the small-scale power spectrum of dark matter. In our hidden charged dark matter scenario, the relevant interactions are elastic scattering off both hidden sector photons and neutrinos. For simplicity of presentation, we present results below for just Compton scattering off of photons. This is the dominant process in most of parameter space. In our numerical analysis and the results presented above, however, we include also the neutrino scattering process.

The cross section for Compton scattering is

$$\sigma_{\tilde{\tau}^h\gamma^h} = \frac{8\pi\alpha_X^2}{3m_X^2} \ . \tag{A.1}$$

This differs markedly from the usual WIMP interaction cross section with standard model fermions, which is suppressed relative to this by $(T/m_\chi)^2$. This would result in lower decoupling temperatures although the effect is mitigated to a large extent by the smaller coupling required to obtain the correct relic abundance, as discussed in section 3.

We study the Fourier-decomposed perturbations in the conformal Newtonian gauge. See ref. [128] for details. For this purpose it is better to use the visible photon temperature T as the "clock." Different hidden sector reheating temperatures $T^h_{\mathrm{RH}} = \xi_{\mathrm{RH}}\, T_{\mathrm{RH}}$ result in very different dark matter kinetic decoupling temperatures T_{kd} (cf. figure 2). However, their effect on the relation of the conformal time $\eta \equiv \int dt/a(t)$ to the visible photon temperature is small.

For simplicity we assume that the fluctuation of the gravitational potential is determined solely by the visible sector photons because the energy density of the visible sector dominates. With this approximation we may use the analytic result for the Newtonian potential in the radiation dominated regime,

$$\Phi = 3\Phi_P \left[\frac{\sin(k\eta/\sqrt{3}) - (k\eta/\sqrt{3})\,\cos(k\eta/\sqrt{3})}{(k\eta/\sqrt{3})^3}\right] , \tag{A.2}$$

where k is the Fourier mode of interest and Φ_P is the primordial amplitude. This approximation results in $\lesssim 10\%$ error, depending on ξ_{RH}. The γ^h perturbations may be expanded

JCAP07(2009)004

in Legendre polynomials and this decomposition results in a multipole hierarchy:

$$\begin{aligned}
\dot{\Theta}^h_0 + k\Theta^h_1 &= -\dot{\Phi} \\
\dot{\Theta}^h_1 + k\left(\frac{2}{3}\Theta^h_2 - \frac{1}{3}\Theta^h_0\right) &= \frac{k\Psi}{3} - \dot{\tau}\left(\Theta^h_1 - \frac{\theta_X}{3k}\right) \\
\dot{\Theta}^h_2 - \frac{2k}{5}\Theta^h_1 &= -\frac{9}{10}\dot{\tau}\Theta^h_2 \\
\dot{\Theta}^h_l &= \frac{k}{2l+1}\left[l\,\Theta^h_{l-1} - (l+1)\,\Theta^h_{l+1}\right] - \dot{\tau}\,\Theta^h_l \quad \text{for } l \geq 3\,,
\end{aligned} \tag{A.3}$$

where the Θ^h_l are the multipole moments of the hidden sector temperature field, to a good approximation $\Psi = -\Phi$, $\dot{\tau} \equiv a\, n_X\, \sigma_{\tilde{\tau}^h\gamma^h}$ is the scattering rate, and n_X is the $\tilde{\tau}^h$ number density. The dark matter density and velocity perturbations are

$$\begin{aligned}
\dot{\delta}_X + \theta_X &= -3\dot{\Phi} \\
\dot{\theta}_X + \frac{\dot{a}}{a}\,\theta_X &= -k^2\Phi + k^2 c_s^2\,\delta_X - k^2\sigma_X + \frac{3\dot{\tau}}{R}\left(k\Theta^h_1 - \frac{\theta_X}{3}\right)\,,
\end{aligned} \tag{A.4}$$

where $R \equiv 3\rho_X/4\rho_{\gamma^h}$ is the ratio of dark matter to hidden sector photon energy density. The interaction term

$$\frac{3\dot{\tau}}{R} = \frac{32\pi^3\alpha_X^2}{45}\frac{T^{h\,4}}{m_X^3}a \tag{A.5}$$

is the rate of transferring momentum $|\vec{p}| \sim T^h$ from the hidden sector photons to the dark matter particles (cf. the second term in eq. (3.8)). We follow the treatment in ref. [52] to set the dark matter sound speed c_s and shear σ_X.

The main difference between our hidden sector scenario and standard cosmology is that the hidden sector photon decoupling epoch is much earlier than the drag epoch of the hidden charged dark matter. We include hidden sector photon higher multipoles and truncate the series at $l_{\rm max} = 10$ to accurately account for the free-streaming of photons.

To obtain the transfer function we solve the dark matter fluid equation well into the decoupling regime and the evolve further in time (when the calculation becomes computationally intensive) using the free-streaming solution [52]

$$\delta_X(\eta) = \exp\left[-\frac{1}{2}\frac{k^2}{k_f^2}\ln^2\left(\frac{\eta}{\eta_*}\right)\right]\left[\delta_X|_{\eta_*} + \left.\frac{d\delta_X}{d\eta}\right|_{\eta_*}\eta_*\ln\left(\frac{\eta}{\eta_*}\right)\right], \tag{A.6}$$

where $k_f^{-2} = \eta_*^2 T^h(\eta_*)/m_X$, to the time of matter-radiation equality.

References

[1] I.Y. Kobsarev, L.B. Okun and I.Y. Pomeranchuk, *On the possibility of observing mirror particles*, *Sov. J. Nucl. Phys.* **3** (1966) 837 [*Yad. Fiz.* **3** (1966) 1154].

[2] S.I. Blinnikov and M.Y. Khlopov, *On possible effects of 'mirror' particles*, *Sov. J. Nucl. Phys.* **36** (1982) 472 [*Yad. Fiz.* **36** (1982) 809] [SPIRES]; *Possible astronomical effects of mirror particles*, *Sov. Astron.* **27** (1983) 371 [*Astron. Zh.* **60** (1983) 632].

[3] H.M. Hodges, *Mirror baryons as the dark matter*, *Phys. Rev.* **D 47** (1993) 456 [SPIRES].

JCAP07(2009)004

[4] Z.G. Berezhiani, A.D. Dolgov and R.N. Mohapatra, *Asymmetric inflationary reheating and the nature of mirror universe*, *Phys. Lett.* **B 375** (1996) 26 [hep-ph/9511221] [SPIRES].

[5] R.N. Mohapatra and V.L. Teplitz, *Mirror dark matter and galaxy core densities*, *Phys. Rev.* **D 62** (2000) 063506 [astro-ph/0001362] [SPIRES].

[6] Z. Berezhiani, D. Comelli and F.L. Villante, *The early mirror universe: inflation, baryogenesis, nucleosynthesis and dark matter*, *Phys. Lett.* **B 503** (2001) 362 [hep-ph/0008105] [SPIRES].

[7] R.N. Mohapatra, S. Nussinov and V.L. Teplitz, *Mirror matter as self interacting dark matter*, *Phys. Rev.* **D 66** (2002) 063002 [hep-ph/0111381] [SPIRES].

[8] A.Y. Ignatiev and R.R. Volkas, *Mirror dark matter and large scale structure*, *Phys. Rev.* **D 68** (2003) 023518 [hep-ph/0304260] [SPIRES].

[9] R. Foot, *Implications of the DAMA and CRESST experiments for mirror matter-type dark matter*, *Phys. Rev.* **D 69** (2004) 036001 [hep-ph/0308254] [SPIRES].

[10] Z. Berezhiani, P. Ciarcelluti, D. Comelli and F.L. Villante, *Structure formation with mirror dark matter: CMB and LSS*, *Int. J. Mod. Phys.* **D 14** (2005) 107 [astro-ph/0312605] [SPIRES].

[11] R. Foot and R.R. Volkas, *Spheroidal galactic halos and mirror dark matter*, *Phys. Rev.* **D 70** (2004) 123508 [astro-ph/0407522] [SPIRES].

[12] J.L. Feng and J. Kumar, *The WIMPless miracle: dark-matter particles without weak-scale masses or weak interactions*, *Phys. Rev. Lett.* **101** (2008) 231301 [arXiv:0803.4196] [SPIRES].

[13] J.L. Feng, J. Kumar and L.E. Strigari, *Explaining the DAMA signal with WIMPless dark matter*, *Phys. Lett.* **B 670** (2008) 37 [arXiv:0806.3746] [SPIRES].

[14] J.L. Feng, J. Kumar, J. Learned and L.E. Strigari, *Testing the dark matter interpretation of the DAMA/LIBRA result with super-kamiokande*, *JCAP* **01** (2009) 032 [arXiv:0808.4151] [SPIRES].

[15] J. Kumar, *From DAMA/LIBRA to super-kamiokande*, arXiv:0903.1700 [SPIRES].

[16] J.L. Feng, H. Tu and H.-B. Yu, *Thermal relics in hidden sectors*, *JCAP* **10** (2008) 043 [arXiv:0808.2318] [SPIRES].

[17] D. McKeen, *WIMPless dark matter and meson decays with missing energy*, arXiv:0903.4982 [SPIRES].

[18] A. Ibarra, A. Ringwald and C. Weniger, *Hidden gauginos of an unbroken* U(1)*: cosmological constraints and phenomenological prospects*, *JCAP* **01** (2009) 003 [arXiv:0809.3196] [SPIRES].

[19] L. Ackerman, M.R. Buckley, S.M. Carroll and M. Kamionkowski, *Dark matter and dark radiation*, *Phys. Rev.* **D 79** (2009) 023519 [arXiv:0810.5126] [SPIRES].

[20] N. Kaloper and A. Padilla, *Levitating dark matter*, arXiv:0904.2394 [SPIRES].

[21] D.-C. Dai, K. Freese and D. Stojkovic, *Constraints on dark matter particles charged under a hidden gauge group from primordial black holes*, arXiv:0904.3331 [SPIRES].

[22] T. Han and R. Hempfling, *Messenger sneutrinos as cold dark matter*, *Phys. Lett.* **B 415** (1997) 161 [hep-ph/9708264] [SPIRES].

[23] E.A. Baltz and H. Murayama, *Gravitino warm dark matter with entropy production*, *JHEP* **05** (2003) 067 [astro-ph/0108172] [SPIRES].

[24] M. Ibe and R. Kitano, *Gauge mediation in supergravity and gravitino dark matter*, *Phys. Rev.* **D 75** (2007) 055003 [hep-ph/0611111] [SPIRES].

[25] J.L. Feng, B.T. Smith and F. Takayama, *Goldilocks supersymmetry: simultaneous solution to dark matter and flavor problems of supersymmetry*, *Phys. Rev. Lett.* **100** (2008) 021302 [arXiv:0709.0297] [SPIRES].

JCAP07(2009)004

[26] D. Hooper and K.M. Zurek, *Natural supersymmetric model with MeV dark matter*, *Phys. Rev.* **D 77** (2008) 087302 [arXiv:0801.3686] [SPIRES].

[27] H. Pagels and J.R. Primack, *Supersymmetry, cosmology and new TeV physics*, *Phys. Rev. Lett.* **48** (1982) 223 [SPIRES].

[28] A. Sommerfeld, *Die Reibung, Wärmeleitung und Diffusion in Gasmischungen XIX. Temperaturkoeffizient, Zahlwert und Vorausberechnung der Gasreibung aus chemischer Formel und kritischer Temperatur* (in German), *Annalen Phys.* **403** (1931) 207.

[29] X.-l. Chen, M. Kamionkowski and X.-m. Zhang, *Kinetic decoupling of neutralino dark matter*, *Phys. Rev.* **D 64** (2001) 021302 [astro-ph/0103452] [SPIRES].

[30] V. Berezinsky, V. Dokuchaev and Y. Eroshenko, *Small-scale clumps in the galactic halo and dark matter annihilation*, *Phys. Rev.* **D 68** (2003) 103003 [astro-ph/0301551] [SPIRES].

[31] A.M. Green, S. Hofmann and D.J. Schwarz, *The power spectrum of SUSY-CDM on sub-galactic scales*, *Mon. Not. Roy. Astron. Soc.* **353** (2004) L23 [astro-ph/0309621] [SPIRES].

[32] M. Kamionkowski and S. Profumo, *Early annihilation and diffuse backgrounds in models of weakly interacting massive particles in which the cross section for pair annihilation is enhanced by* $1/V$, *Phys. Rev. Lett.* **101** (2008) 261301 [arXiv:0810.3233] [SPIRES].

[33] S.W. Randall, M. Markevitch, D. Clowe, A.H. Gonzalez and M. Bradac, *Constraints on the self-interaction cross-section of dark matter from numerical simulations of the merging galaxy cluster* $1E0657-5$, arXiv:0704.0261 [SPIRES].

[34] J. Miralda-Escude, *A test of the collisional dark matter hypothesis from cluster lensing*, astro-ph/0002050 [SPIRES].

[35] M. Pospelov, A. Ritz and M.B. Voloshin, *Secluded WIMP dark matter*, *Phys. Lett.* **B 662** (2008) 53 [arXiv:0711.4866] [SPIRES].

[36] J. Jaeckel, J. Redondo and A. Ringwald, *Signatures of a hidden cosmic microwave background*, *Phys. Rev. Lett.* **101** (2008) 131801 [arXiv:0804.4157] [SPIRES].

[37] W. Krolikowski, *Again on hidden sector of the universe, accessible through photonic portal*, *Acta Phys. Polon.* **B 40** (2009) 111 [arXiv:0809.1931] [SPIRES].

[38] N. Arkani-Hamed, D.P. Finkbeiner, T.R. Slatyer and N. Weiner, *A theory of dark matter*, *Phys. Rev.* **D 79** (2009) 015014 [arXiv:0810.0713] [SPIRES].

[39] S. Gardner, *Shedding light on dark matter: a Faraday rotation experiment to limit a dark magnetic moment*, *Phys. Rev.* **D 79** (2009) 055007 [arXiv:0811.0967] [SPIRES].

[40] E.J. Chun and J.-C. Park, *Dark matter and sub-GeV hidden* U(1) *in GMSB models*, *JCAP* **02** (2009) 026 [arXiv:0812.0308] [SPIRES].

[41] J.D. March-Russell and S.M. West, *WIMPonium and boost factors for indirect dark matter detection*, *Phys. Lett.* **B 676** (2009) 133 [arXiv:0812.0559] [SPIRES].

[42] M. Baumgart, C. Cheung, J.T. Ruderman, L.-T. Wang and I. Yavin, *Non-abelian dark sectors and their collider signatures*, *JHEP* **04** (2009) 014 [arXiv:0901.0283] [SPIRES].

[43] W. Shepherd, T.M.P. Tait and G. Zaharijas, *WIMPonium*, arXiv:0901.2125 [SPIRES].

[44] C. Cheung, J.T. Ruderman, L.-T. Wang and I. Yavin, *Kinetic mixing as the origin of light dark scales*, arXiv:0902.3246 [SPIRES].

[45] A. Katz and R. Sundrum, *Breaking the dark force*, *JHEP* **06** (2009) 003 [arXiv:0902.3271] [SPIRES].

[46] B. Batell, M. Pospelov and A. Ritz, *Probing a secluded* U(1) *at B-factories*, arXiv:0903.0363 [SPIRES].

[47] R. Essig, P. Schuster and N. Toro, *Probing dark forces and light hidden sectors at low-energy* e^+e^- *colliders*, arXiv:0903.3941 [SPIRES].

JCAP07(2009)004

[48] S. Gopalakrishna, S.J. Lee and J.D. Wells, *Dark matter and Higgs boson collider implications of fermions in an abelian-gauged hidden sector*, arXiv:0904.2007 [SPIRES].

[49] D.E. Morrissey, D. Poland and K.M. Zurek, *Abelian hidden sectors at a GeV*, arXiv:0904.2567 [SPIRES].

[50] X.-J. Bi et al., *Non-thermal production of WIMPs, cosmic $e^{\pm}$ excesses and γ-rays from the galactic center*, arXiv:0905.1253 [SPIRES].

[51] A.M. Green, S. Hofmann and D.J. Schwarz, *The first WIMPy halos*, *JCAP* **08** (2005) 003 [astro-ph/0503387] [SPIRES].

[52] A. Loeb and M. Zaldarriaga, *The small-scale power spectrum of cold dark matter*, *Phys. Rev.* **D 71** (2005) 103520 [astro-ph/0504112] [SPIRES].

[53] S. Profumo, K. Sigurdson and M. Kamionkowski, *What mass are the smallest protohalos?*, *Phys. Rev. Lett.* **97** (2006) 031301 [astro-ph/0603373] [SPIRES].

[54] E. Bertschinger, *The effects of cold dark matter decoupling and pair annihilation on cosmological perturbations*, *Phys. Rev.* **D 74** (2006) 063509 [astro-ph/0607319] [SPIRES].

[55] T. Bringmann and S. Hofmann, *Thermal decoupling of WIMPs from first principles*, *JCAP* **07** (2007) 016 [hep-ph/0612238] [SPIRES].

[56] D. Hooper, M. Kaplinghat, L.E. Strigari and K.M. Zurek, *MeV dark matter and small scale structure*, *Phys. Rev.* **D 76** (2007) 103515 [arXiv:0704.2558] [SPIRES].

[57] M. Kaplinghat, *Dark matter from early decays*, *Phys. Rev.* **D 72** (2005) 063510 [astro-ph/0507300] [SPIRES].

[58] J.A.R. Cembranos, J.L. Feng, A. Rajaraman and F. Takayama, *SuperWIMP solutions to small scale structure problems*, *Phys. Rev. Lett.* **95** (2005) 181301 [hep-ph/0507150] [SPIRES].

[59] A. Pukhov et al., *CompHEP: a package for evaluation of Feynman diagrams and integration over multi-particle phase space. User's manual for version* 33, hep-ph/9908288 [SPIRES].

[60] A. Pukhov, *CalcHEP* 3.2*: mSSM, structure functions, event generation, batchs and generation of matrix elements for other packages*, hep-ph/0412191 [SPIRES].

[61] J. Hisano, K.T. Inoue and T. Takahashi, *Constraining superWIMPy and warm subhalos with future submillilensing*, *Phys. Lett.* **B 643** (2006) 141 [hep-ph/0608126] [SPIRES].

[62] J. Diemand, B. Moore and J. Stadel, *Earth-mass dark-matter haloes as the first structures in the early universe*, *Nature* **433** (2005) 389 [astro-ph/0501589] [SPIRES].

[63] S. Ando and E. Komatsu, *Anisotropy of the cosmic gamma-ray background from dark matter annihilation*, *Phys. Rev.* **D 73** (2006) 023521 [astro-ph/0512217] [SPIRES].

[64] S.M. Koushiappas, *Proper motion of gamma-rays from microhalo sources*, *Phys. Rev. Lett.* **97** (2006) 191301 [astro-ph/0606208] [SPIRES].

[65] S. Ando, E. Komatsu, T. Narumoto and T. Totani, *Dark matter annihilation or unresolved astrophysical sources? Anisotropy probe of the origin of cosmic gamma-ray background*, *Phys. Rev.* **D 75** (2007) 063519 [astro-ph/0612467] [SPIRES].

[66] A. Cuoco, J. Brandbyge, S. Hannestad, T. Haugboelle and G. Miele, *Angular signatures of annihilating dark matter in the cosmic gamma-ray background*, *Phys. Rev.* **D 77** (2008) 123518 [arXiv:0710.4136] [SPIRES].

[67] S. Ando, M. Kamionkowski, S.K. Lee and S.M. Koushiappas, *Can proper motions of dark-matter subhalos be detected?*, *Phys. Rev.* **D 78** (2008) 101301 [arXiv:0809.0886] [SPIRES].

[68] J.M. Siegal-Gaskins, *Revealing dark matter substructure with anisotropies in the diffuse gamma-ray background*, *JCAP* **10** (2008) 040 [arXiv:0807.1328] [SPIRES].

[69] S.K. Lee, S. Ando and M. Kamionkowski, *The gamma-ray-flux probability distribution function from galactic halo substructure*, arXiv:0810.1284 [SPIRES].

JCAP07(2009)004

[70] J. Hisano, S. Matsumoto and M.M. Nojiri, *Unitarity and higher-order corrections in neutralino dark matter annihilation into two photons*, *Phys. Rev.* **D 67** (2003) 075014 [hep-ph/0212022] [SPIRES].

[71] J. Hisano, S. Matsumoto and M.M. Nojiri, *Explosive dark matter annihilation*, *Phys. Rev. Lett.* **92** (2004) 031303 [hep-ph/0307216] [SPIRES].

[72] J. Hisano, S. Matsumoto, M.M. Nojiri and O. Saito, *Non-perturbative effect on dark matter annihilation and gamma ray signature from galactic center*, *Phys. Rev.* **D 71** (2005) 063528 [hep-ph/0412403] [SPIRES].

[73] M. Cirelli, A. Strumia and M. Tamburini, *Cosmology and astrophysics of minimal dark matter*, *Nucl. Phys.* **B 787** (2007) 152 [arXiv:0706.4071] [SPIRES].

[74] H.A. Bethe and E.E. Salpeter, *Quantum mechanics of one- and two-electron atoms*, Springer-Verlag, Berlin Göttingen Heidelberg Germany (1957).

[75] J.F. Navarro, C.S. Frenk and S.D.M. White, *A universal density profile from hierarchical clustering*, *Astrophys. J.* **490** (1997) 493 [astro-ph/9611107] [SPIRES].

[76] J. Diemand, M. Kuhlen and P. Madau, *Early supersymmetric cold dark matter substructure*, *Astrophys. J.* **649** (2006) 1 [astro-ph/0603250] [SPIRES].

[77] WMAP collaboration, E. Komatsu et al., *Five-year Wilkinson Microwave Anisotropy Probe (WMAP) observations: cosmological interpretation*, *Astrophys. J. Suppl.* **180** (2009) 330 [arXiv:0803.0547] [SPIRES].

[78] M. Kaplinghat, L. Knox and M.S. Turner, *Annihilating the cold dark matter cusp crisis*, *Phys. Rev. Lett.* **85** (2000) 3335 [astro-ph/0005210] [SPIRES].

[79] R. Dave, D.N. Spergel, P.J. Steinhardt and B.D. Wandelt, *Halo properties in cosmological simulations of self-interacting cold dark matter*, *Astrophys. J.* **547** (2001) 574 [astro-ph/0006218] [SPIRES].

[80] N. Yoshida, V. Springel, S.D.M. White and G. Tormen, *Collisional dark matter and the structure of dark halos*, *Astrophys. J.* **535** (2000) L103 [astro-ph/0002362] [SPIRES].

[81] D.A. Buote, T.E. Jeltema, C.R. Canizares and G.P. Garmire, *Chandra evidence for a flattened, triaxial dark matter halo in the elliptical galaxy NGC720*, *Astrophys. J.* **577** (2002) 183 [astro-ph/0205469] [SPIRES].

[82] P. Humphrey et al., in preparation.

[83] T. Fang, P.J. Humphrey and D.A. Buote, *Rotation and turbulence of the hot ICM in galaxy clusters*, *Astrophys. J.* **691** (2009) 1648 [arXiv:0808.1106] [SPIRES].

[84] D.N. Spergel and P.J. Steinhardt, *Observational evidence for self-interacting cold dark matter*, *Phys. Rev. Lett.* **84** (2000) 3760 [astro-ph/9909386] [SPIRES].

[85] B. Moore, *Evidence against dissipationless dark matter from observations of galaxy haloes*, *Nature* **370** (1994) 629 [SPIRES].

[86] B. Moore, T.R. Quinn, F. Governato, J. Stadel and G. Lake, *Cold collapse and the core catastrophe*, *Mon. Not. Roy. Astron. Soc.* **310** (1999) 1147 [astro-ph/9903164] [SPIRES].

[87] W.J.G. de Blok and S.S. McGaugh, *The dark and baryonic matter content of low surface brightness disk galaxies*, *Mon. Not. Roy. Astron. Soc.* **290** (1997) 533 [astro-ph/9704274] [SPIRES].

[88] A.A. Klypin, A.V. Kravtsov, O. Valenzuela and F. Prada, *Where are the missing galactic satellites?*, *Astrophys. J.* **522** (1999) 82 [astro-ph/9901240] [SPIRES].

[89] B. Moore et al., *Dark matter substructure within galactic halos*, *Astrophys. J.* **524** (1999) L19 [SPIRES].

[90] L.E. Strigari et al., *Redefining the missing satellites problem*, arXiv:0704.1817 [SPIRES].

[91] E.J. Tollerud, J.S. Bullock, L.E. Strigari and B. Willman, *Hundreds of milky way satellites? Luminosity bias in the satellite luminosity function*, arXiv:0806.4381 [SPIRES].

JCAP07(2009)004

[92] J.D. Simon, A.D. Bolatto, A. Leroy, L. Blitz and E.L. Gates, *High-resolution measurements of the halos of four dark matter-dominated galaxies: deviations from a universal density profile*, *Astrophys. J.* **621** (2005) 757 [astro-ph/0412035] [SPIRES].

[93] G. Gentile, P. Salucci, U. Klein, D. Vergani and P. Kalberla, *The cored distribution of dark matter in spiral galaxies*, *Mon. Not. Roy. Astron. Soc.* **351** (2004) 903 [astro-ph/0403154] [SPIRES].

[94] G. Gentile, A. Burkert, P. Salucci, U. Klein and F. Walter, *The dwarf galaxy DDO* 47*: testing cusps hiding in triaxial halos*, *Astrophys. J.* **634** (2005) L145 [astro-ph/0510607] [SPIRES].

[95] M. Spano et al., *GHASP: an Hα kinematic survey of spiral and irregular galaxies. V. Dark matter distribution in* 36 *nearby spiral galaxies*, *Mon. Not. Roy. Astron. Soc.* **383** (2008) 297 [arXiv:0710.1345] [SPIRES].

[96] R. Kuzio de Naray, S.S. McGaugh and W.J.G. de Blok, *Mass models for low surface brightness galaxies with high resolution optical velocity fields*, *Astrophys. J.* **676** (2008) 920 [arXiv:0712.0860] [SPIRES].

[97] B.D. Wandelt et al., *Self-interacting dark matter*, astro-ph/0006344 [SPIRES].

[98] K.-J. Ahn and P.R. Shapiro, *Formation and evolution of the self-interacting dark matter halos*, *Mon. Not. Roy. Astron. Soc.* **363** (2005) 1092 [astro-ph/0412169] [SPIRES].

[99] S. Hannestad, *Galactic halos of self-interacting dark matter*, astro-ph/9912558 [SPIRES].

[100] N. Yoshida, V. Springel, S.D.M. White and G. Tormen, *Weakly self-interacting dark matter and the structure of dark halos*, *Astrophys. J.* **544** (2000) L87 [astro-ph/0006134] [SPIRES].

[101] B. Moore, S. Gelato, A. Jenkins, F.R. Pearce and V. Quilis, *Collisional versus collisionless dark matter*, *Astrophys. J.* **535** (2000) L21 [astro-ph/0002308] [SPIRES].

[102] M.W. Craig and M. Davis, *The structure of dark matter halos in an annihilating dark matter model*, astro-ph/0106542 [SPIRES].

[103] C.S. Kochanek and M.J. White, *A quantitative study of interacting dark matter in halos*, *Astrophys. J.* **543** (2000) 514 [astro-ph/0003483] [SPIRES].

[104] L.V.E. Koopmans, T. Treu, A.S. Bolton, S. Burles and L.A. Moustakas, *The Sloan lens ACS survey. III — the structure and formation of early-type galaxies and their evolution since* $z \sim 1$, *Astrophys. J.* **649** (2006) 599 [astro-ph/0601628] [SPIRES].

[105] SDSS collaboration, N. Inada et al., *A gravitationally lensed quasar with quadruple images separated by* 14.62 *arcseconds*, *Nature* **426** (2003) 810 [astro-ph/0312427] [SPIRES].

[106] T. Morokuma et al., *Discovery of a gravitationally lensed quasar from the Sloan Digital Sky Survey: SDSS J*133222.62 + 034739.9, *Astron. J.* **133** (2007) 214 [astro-ph/0609695] [SPIRES].

[107] A.K.D. Evans and S. Bridle, *A detection of dark matter halo ellipticity using galaxy cluster lensing in SDSS*, *Astrophys. J.* **695** (2009) 1446 [arXiv:0806.2723] [SPIRES].

[108] H. Hoekstra, H.K.C. Yee and M.D. Gladders, *Properties of galaxy dark matter halos from weak lensing*, *Astrophys. J.* **606** (2004) 67 [astro-ph/0306515] [SPIRES].

[109] R. Mandelbaum, C.M. Hirata, T. Broderick, U. Seljak and J. Brinkmann, *Ellipticity of dark matter halos with galaxy-galaxy weak lensing*, *Mon. Not. Roy. Astron. Soc.* **370** (2006) 1008 [astro-ph/0507108] [SPIRES].

[110] O. Host et al., *Measurement of the dark matter velocity anisotropy in galaxy clusters*, *Astrophys. J.* **690** (2009) 358 [arXiv:0808.2049] [SPIRES].

[111] J. Koda, private communication.

[112] P. Colin, V. Avila-Reese, O. Valenzuela and C. Firmani, *The structure of halos in self-interacting cold dark matter models*, *Rev. Mex. Astron. Astrophys.* **17** (2003) 19 [astro-ph/0306327] [SPIRES].

JCAP07(2009)004

[113] C. Firmani, E. D'Onghia, V. Avila-Reese, G. Chincarini and X. Hernandez, *Evidence of self-interacting cold dark matter from galactic to galaxy cluster scales*, *Mon. Not. Roy. Astron. Soc.* **315** (2000) L29 [astro-ph/0002376] [SPIRES].

[114] C. Firmani, E. D'Onghia, G. Chincarini, X. Hernandez and V. Avila-Reese, *Constraints on dark matter physics from dwarf galaxies through galaxy cluster haloes*, *Mon. Not. Roy. Astron. Soc.* **321** (2001) 713 [astro-ph/0005001] [SPIRES].

[115] J.F. Hennawi and J.P. Ostriker, *Observational constraints on the self interacting dark matter scenario and the growth of supermassive black holes*, *Astrophys. J.* **572** (2002) 41 [astro-ph/0108203] [SPIRES].

[116] F.J. Sanchez-Salcedo, *The dark halo of NGC* 5963 *as a constraint on dark matter self-interaction at the low velocity regime*, *Astrophys. J.* **631** (2005) 244 [astro-ph/0506345] [SPIRES].

[117] P.J. Humphrey et al., *A Chandra view of dark matter in early-type galaxies*, *Astrophys. J.* **646** (2006) 899 [astro-ph/0601301] [SPIRES].

[118] P.J. Humphrey, private communication.

[119] O.Y. Gnedin, A. Gould, J. Miralda-Escude and A.R. Zentner, *Probing the shape of the galactic halo with hyper-velocity stars*, *Astrophys. J.* **634** (2005) 344 [astro-ph/0506739] [SPIRES].

[120] A. Vikhlinin et al., *Chandra sample of nearby relaxed galaxy clusters: mass, gas fraction and mass-temperature relation*, *Astrophys. J.* **640** (2006) 691 [astro-ph/0507092] [SPIRES].

[121] C. Trachternach, W.J.G. de Blok, F. Walter, E. Brinks and R.C. Kennicutt, *Dynamical centers and non-circular motions in THINGS galaxies: implications for dark matter halos*, arXiv:0810.2116 [SPIRES].

[122] L.E. Strigari et al., *A common mass scale for satellite galaxies of the Milky Way*, *Nature* **454** (2008) 1096 [arXiv:0808.3772] [SPIRES].

[123] L.E. Strigari et al., *A large dark matter core in the fornax dwarf spheroidal galaxy?*, *Astrophys. J.* **652** (2006) 306 [astro-ph/0603775] [SPIRES].

[124] G. Gilmore et al., *The observed properties of dark matter on small spatial scales*, *Astrophys. J.* **663** (2007) 948 [astro-ph/0703308] [SPIRES].

[125] L.E. Strigari, J.S. Bullock and M. Kaplinghat, *Determining the nature of dark matter with astrometry*, *Astrophys. J.* **657** (2007) L1 [astro-ph/0701581] [SPIRES].

[126] M. Markevitch et al., *Direct constraints on the dark matter self-interaction cross-section from the merging cluster* $1E0657-56$, *Astrophys. J.* **606** (2004) 819 [astro-ph/0309303] [SPIRES].

[127] S.M. Carroll, S. Mantry and M.J. Ramsey-Musolf, *Implications of a scalar dark force for terrestrial experiments*, arXiv:0902.4461 [SPIRES].

[128] C.-P. Ma and E. Bertschinger, *Cosmological perturbation theory in the synchronous and conformal Newtonian gauges*, *Astrophys. J.* **455** (1995) 7 [astro-ph/9506072] [SPIRES].

JCAP07(2009)004